FACULDADE DE ENGENHARIA DA UNIVERSIDADE DO PORTO

A pervasive system for real-time blood pressure monitoring

Pedro Manuel Pinto da Silva

Mestrado Integrado em Engenharia Eletrotécnica e de Computadores

Supervisor: João Paulo Trigeiros da Silva Cunha

July 30, 2013

Resumo

É aceite globalmente que a regulação e monitorização da pressão arterial contribui ativamente para a melhoria da qualidade de vida da população através da prevenção de episódios e doenças cardiovasculares.

Recentemente, apesar terem sido feitos avanços na área da monitorização ambulatória não-invasiva da pressão arterial (MAPA), dispositivos de MAPA ou baseados na tecnologia Finapres trazem custos financeiros e de usabilidade significativos que os impedem de ser usados pela maioria da população numa base diária.

Nos últimos anos, técnicas baseadas no *pulse transit time* (PTT) foram consideradas como um instrumento promissor para monitorizar de forma não-invasiva e contínua a pressão arterial, a um nível personalizado. Neste trabalho aborda-se a questão de como modelos baseados em PTT se comportam como estimadores de pressão arterial sistólica (SBP) através de várias abordagens. Off-line *least squares fitting* e *recursive least squares* são aplicados para determinar a correlação entre os parâmetros do modelo e a sua evolução no tempo. Obtêm-se baixos coeficientes de correlação e não se observa nenhuma evolução sistemática dos parâmetros no tempo. On-line *exponentially-weighted regression* é aplicada, com uma calibração inicial, e uma recalibração do sistema a cada T minutos. Observa-se que desvio padrão do erro e o erro quadrático mínimo aumentam consideravelmente com T, sugerindo que os parâmetros determinados inicialmente se tornam cada mais obsoletos depois de 30 a 60 minutos de atividade.

No entanto, permanece a questão se um modelo baseado em PTT é um indicador de variabilidade de SBP suficientemente bom para detetar eventos de pressão arterial sistólica. Através da imposição de requisitos médicos, nomeadamente um $threshold$ de 20 mmHg para mudanças de SBP significativas, eventos de SBP são definidos e obtidos através de um conjunto de técnicas desenvolvidas. Após a geração o $groundtruth$ (GT), são analisados os $thresholds$ que maximizam os *tradeoffs* entre o número de deteções positivas verdadeiras e falsas através da geração de curvas de performance ROC para três diferentes métodos de estimar a pressão arterial sistólica. Pontos específicos na curva ROC do método *exponentially-weigted regression* com um período de recalibração de 20 minutos, sugeriram que o método pode ser incorporado com tecnologia atual de monitorização de pressão arterial, usando um $threshold$ de 12.5 com $performance$ razoável (82% sensibilidade e 79% especificidade).

Abstract

It is widely spread and accepted that regulation and monitoring of arterial blood pressure contributes actively to the prevention of cardiovascular events and diseases.

Although developments have been made in non-invasive ambulatory blood pressure measurement, ambulatory blood pressure monitors or devices based on Finapres technology carry significant costs or performance drawbacks that do not make them eligible for a widespread use of the technology.

Recently, pulse transit time (PTT) based techniques have been suggested as a promising tool to deliver non-invasive and continuous monitoring of BP on a personalized wearable level. In this work the question of how PTT-based models performs as an estimator of SBP is addressed using several approaches. Off-line least squares fitting and recursive least squares are applied to determine parameter correlation and evolution in time. Low correlation coefficients are found and no systematic components are observed. On-line exponentially-weighted regression is applied by performing an initial calibration and then re-calibrating the system every T minutes. Standard deviation of the error and minimum squared error were observed to increase considerably with T, suggesting that initially determined parameters become increasingly obsolete after 30 to 60 minutes of activity.

However, the question whether a PTT-based model is an indicator of SBP variability strong enough to detect events of SBP remained. By imposing medical requirements, namely a threshold for significant SBP changes of 20 mmHg, SBP events are characterized and a set of techniques for SBP event detection are developed. Upon generating the ground truth, the thresholds that maximize the tradeoffs between the number of true and false positive detections are analysed by generating ROC performance curves for three different methods of estimating SBP. Specific points in the ROC curve of a exponentially-weighted regression with period of re-calibration of 20 minutes suggested that the method could be incorporated with current technology for ambulatory BP measurement using a threshold of $tr = 12.5$ and providing reasonable performance (82% sensibility and 79% specificity).

Acknowledgements

I would like to thank Dr. Vasco Gama and Dr. Daniel Caeiro from the Hospital Center of Vila Nova de Gaia and Espinho for their collaboration in the project, especially in providing relevant physiological acquired data from their patients monitoring station, and for making themselves available to give the most varied medical explanations and clarifications.

I would also like to thank all the RTABP team, originated in IEETA, Aveiro, for making me feel welcome and for their contributions to the project, in particular Luka Mitjovik for his toolbox of physiological data processing, and Susana Brás for diverse clarifications, suggestions and shared material.

I would like, above all, to show my gratitude to my mother for her limitless patience towards me, my demands and tantrums. Without her priceless help in providing and complementing ideas and work references this would not have been possible. I would also like to thank my father for keeping me in line and the rest of my family for their unconditional support. A big hug to all my friends that gave me escape routes and company during the weekends, which helped me give a different look at things whenever an idea or solution was needed.

Finally, I would like to thank my supervisor/coordinator Prof. Dr. João Paulo Cunha for giving me this work opportunity, for following my work regularly, for giving me motivation and strength to go on during the lowest points, and by the many encounters he provided me and others, from meetings with high quality professionals of the most diverse scientific sectors to the weekly meetings of brainstorming and ideas exchange between the members of the BRAINlab team.

Thank you all.

Pedro Manuel Pinto da Silva

"Science can amuse and fascinate us all, but it is engineering that changes the world."

Isaac Asimov

Contents

List of Figures

List of Tables

Abbreviations

ABPM	Ambulatory Blood Pressure Monitoring
AIC	Akaike Information Criterion
AUC	Area Under the Curve
BED	Blood Pressure Event Detector
BP	Blood Pressure
CO	Cardiac Output
CVP	Central Venous Pressure
DBP	Diastolic Blood Pressure
ECG	Electrocardiography
EWR	Exponentially-Weighted Regression
FCT	Fundação Portuguesa para a Ciência e Tecnologia
FEUP	Faculdade de Engenharia da Universidade do Porto
FPR	False Positive Rate
GT	Ground Truth
HGaia	Hospital Center of Vila Nova de Gaia and Espinho
HR	Heart Rate
IEETA	Instituto de Engenharia Electrónica e Telemática de Aveiro
ICU	Intensive Care Unit
LSF	Least Squares Fitting
MAP	Mean Arterial Pressure
MIMIC	Multiparameter Intelligent Monitoring in Intensive Care
MSE	Minimum Squared Error
PAT	Pulse Arrival Time
PEP	Pre-Ejection Time
PPG	Photoplethysmography
PTT	Pulse Transit Time
PWV	Pulse Wave Velocity
RLS	Recursive Least Squares
ROC	Receiver Operating Characteristic
SBP	Systolic Blood Pressure
SVR	Systemic Vascular Resistance
VJ	Vital Jacket®
TPR	True Positive Rate

Chapter 1

Introduction

1.1 Work context

This report presents in detail the work developed by student Pedro Manuel Pinto da Silva as the final project of the Master's course in Electrical Engineering and Computers of the Faculty of Engineering of the University of Porto (FEUP), Portugal. It is connected to the project *RTABP - Real Time Arterial Blood Pressure*, which started off in the Engineering Institute of Electronics and Telematics of Aveiro (IEETA). After two accepted publications, in the 2011 6th Iberian Conference [1], and the 2011 Annual International Conference of the IEEE [2], the project is currently not funded by the Portuguese foundation for Science and Technology (FCT), but it has been advancing thanks to progresses made by interested members of the team and recruited students.

More recently, a connection with Hospital Center of Gaia and Espinho (HGaia) has been established, with the purpose of setting up a physiological signal acquisition and monitoring network, which enabled the gathering of relevant data used in the study of cardiovascular related models, namely ones that can estimate BP non-invasively. Under proper supervision, the acquisition of such data combined with clinical information provided by the medical staff, lead by Dr. Vasco Gama, may help in detecting patterns and associations that might have previously passed unnoticed and may prove to be determinant in the development of more accurate BP estimation models. Yet, the process of developing a database of proportions large enough to make such breakthroughs possible takes time, and few cases have been included in this dissertation.

The work here exposed tries to give a contribution to the work already developed by Susana Brás, Óscar Pereira and Paulo Azevedo from IEETA, internship student Luka Mijatovic, and Prof. Dr. João Paulo Cunha.

1.2 Background and motivation

By 2012, cardiovascular diseases represented nearly 50% of the world's cause of death by non-communicable disease [3]. It is well documented the importance of the role played by blood pressure (BP) when it comes to assess the state of the cardiovascular system [4]. In fact, BP is

considered to be a very important indicator of a person's well being, as it provides valuable information on the functional status of the heart and arteries. Therefore, it is widely spread and accepted that regulation and monitoring of arterial blood pressure contributes actively to the prevention of cardiovascular events and diseases.

However, traditional methods and instruments for measuring and monitoring blood pressure, in clinics or at home, are limited to snapshots of systolic and diastolic blood pressure at intervals [5]. Although these methods provide a way to track one's blood pressure, there is far more information of medical interest available in the arterial blood pressure wave, particularly in the systolic blood pressure (SBP) curve. Actually, BP is also known to be a very unstable parameter and its variability alone is considered by some to be a separate risk factor itself [4, 6]. Hence, traditional methods often fail in accounting for cardiovascular events and diseases connected with high variability of BP. Additionally, it has been suggested that visit-to-visit (between medical visits) variability in SBP over periods of time longer than 24 hours may have greater prognostic value than average BP values or short-term variability [6, 7, 8]. For instance, visit-to-visit SBP variability has shown to be a strong predictor of stroke in patients with treated hypertension and patients that previously suffered a transient ischaemic attack (TIA), independently of their mean value of SBP [8].

On the other hand, recent developments have been made in non-invasive ambulatory BP measurement. These are commercially available in the form of personal devices and allow a more complete BP tracking and mapping. Examples of such devices are the Portapres measurement device which enables the recording of a 24 hour blood pressure profile on a beat-to-beat basis, using a finger placed sensor and producing a continuous BP waveform [9]. Ambulatory blood pressure monitoring (ABPM) devices measure BP at regular intervals and usually also used over periods of 24 hours. ABPM devices are believed to be able to reduce the *white coat effect*: people whose BP readings at clinical visits are often higher than home readings, due to anxiety and stress caused by clinical settings [4].

Yet, these devices have significant drawbacks that do not allow them to perform well enough for a widespread use of the technology. Finapres technology has shown performance problems linked with underestimation and noise produced by motion artefacts, and its finger cuff is known to cause transient pain and numbing sensations if used for consecutive hours on the same finger [4, 9]. On the other hand, ABPM devices lack the continuous ambulatory characteristic, strongly limiting their performance and measurement capacities. In addition, the arm cuffs utilized limit their portability and damage their usability. In overall, these devices provide a non-invasive way of understanding how a person's BP changes throughout the day, but their use remains uncomfortable and unreliable for long periods of time and is usually not carried out through consecutive days. Furthermore, the equipment is considered expensive to be acquired in full or rented on a daily basis by most people.

Consequently, the development of an alternative non-invasive and ambulatory system for continuously monitoring BP, which at the same time is comfortable and reliable, would provide deeper insight and understanding of the underlying mechanisms behind blood pressure variability. More importantly, the everyday use of an easy-to-manage and cheaper device would constitute a pow-

erful tool in predicting the trigger of serious cardiovascular events and in helping doctors make anti-hypertensive therapy decisions [10].

On a different level, wearable technology has seen significant advances over the last years, mainly in accurately recording and processing electrocardiographic (ECG) signals. Through analysis of the acquired ECG data, good indicators of stress and fatigue of the monitored individual can be obtained [1]. Integrating this system with the acquisition of plethysmographic (PPG) signals, it would be possible to indirectly estimate BP, using the pulse transit time (PTT). Wearable devices have shown to be a reliable and comfortable way of monitoring patients over extensive periods of time. These systems combine monitoring, display, treatment and alarm functions through the application of wireless technology [11]. This was possible as a result of technical improvements in wireless technologies, which in turn allowed the monitoring of multiple parameters of individuals in parallel. Mobile devices, on the other hand, have presented themselves as a cheaper, but powerful and accessible tool to be used as a monitoring system [12].

Therefore, wearable technology has proved itself to be a very promising mean to deliver continuous non-invasive blood pressure measurement in a comfortable and faithful way. Implementing this functionality in addiction to the ones already in use would result in a true wearable continuous monitoring system that can watch over several important vital signs non-invasively, ultimately being a significant medium to prevent cardiovascular associated diseases and, thus improve life expectancy worldwide.

1.3 Goals and objectives

This work aims at giving a contribution to continuous non-invasive blood pressure estimation using a pulse transit time based approach. Its main goal is to study and provide deeper insight into the models and equations currently used in the literature for this purpose. The models will be explored by varying its parameters and through application of regressive and recursive mathematical techniques. For this, data recordings of patients with relevant cardiovascular characteristics or pathologies will be obtained and used from trustworthy signal databases, particularly the Physionet MIMIC-II (Multiparameter Intelligent Monitoring in Intensive Care) research database [13, 14]. Also, a study on the impact of the calibration process on performance and usability will be performed, in order to search for a point of equilibrium between functional and non-functional requirements of the system.

From the findings and conclusions drawn from previous analysis, an application able to point at certain BP relevant events is to be designed in conformity with the characteristics of a PTT based BP estimation approach. In conference with Dr. Vasco Gama and Dr. Daniel Caeiro at HGaia, a definition of BP event is to be obtained and used as basic criteria for evaluation and detection algorithms under development. Additionally, a technique of detection of structural changes on time series data is to be used, based on literature. Finally, performance graphs will be obtained and evaluated, using receiver-operation-characteristic (ROC) graphs and curves, by varying the

threshold of the main detection parameter. Several graphs or curves may be obtained in respect to the different combination of inputs when estimating BP using PTT.

Ultimately, the contribution of this work will be assessed in overall and towards similar works. Future milestones, outcome paths and possibilities, directly or indirectly resulting from accomplishments made, will be described in detail, accordingly.

1.4 Work tools

The MATLAB® environment is the main tool for design and development used in this work. Additionally, it uses a toolbox for processing the physiological data yielded in the records and obtain the PTT, HR and invasive SBP signals studied in this work.

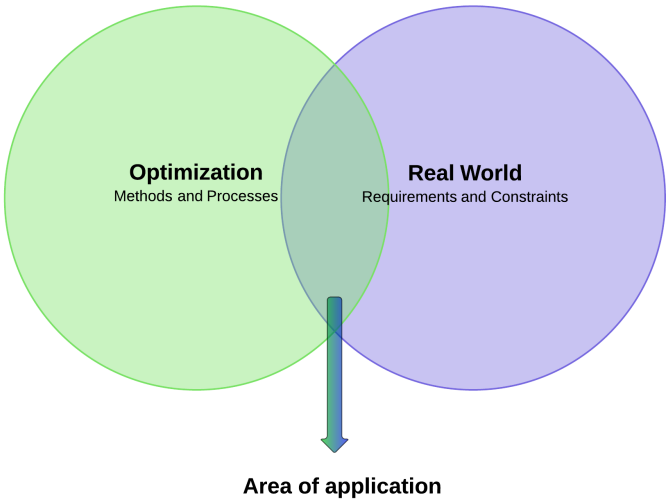

Figure 1.1: Optimization versus real world constraints.

Figure 1.1 represents the paradigm approached in this work. A model for non-invasive BP estimation is studied and are applied optimization methods and processes with scope not limited by boundaries of the real world. Thus, the area of application of this model lies in the space where the results obtained from optimization meet real world requirements and constraints.

Data collection setup

The connections previously established between the RTABP team and the medical team at HGaia, led by Dr. Vasco Gama, resulted in the permission to access a monitoring network set up within an infirmary based on the cardiovascular wing of the hospital. This enabled the access to data of intra-arterial BP, PPG, and ECG being monitored in patients at the infirmary.

The work flow, main interactions and parties involved in this process are represented in Fig. 1.2. Monitoring of patients is performed on a daily basis, but whenever a patient of cardiovascular interest is identified, i.e. a person with cardiovascular pathologies or events that make him or her eligible for ambulatory BP monitoring, the person in charge of supervising the monitoring at HGaia, contacts the person on the RTABP team in charge of collecting the data in order to

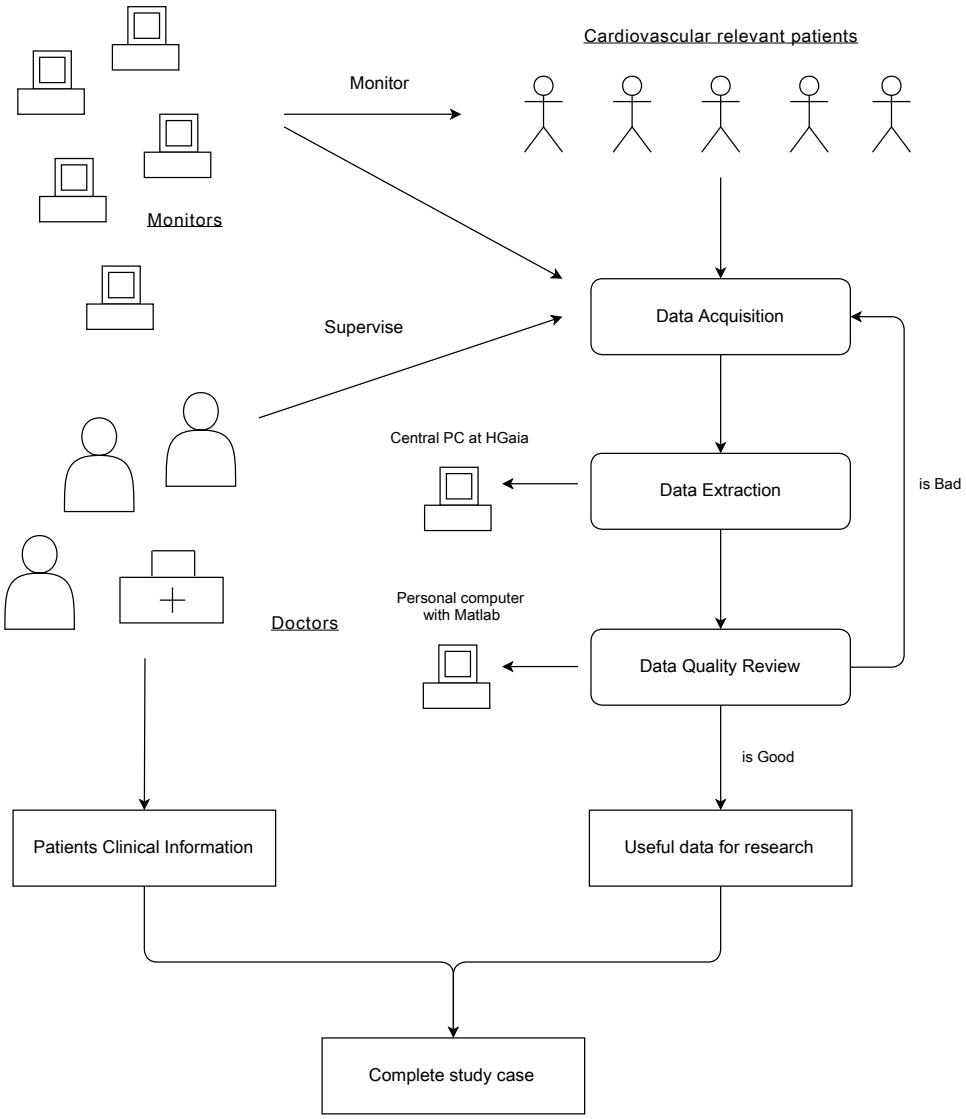

Figure 1.2: Data acquisition setup at HGaia.

trigger the data acquisition process. That includes using special software on a specific computer located at HGaia to acquire the data being monitored in real-time. Once the acquisition is finished, usually lasting between one and two hours, the data is anonymized and extracted to a special format and transferred to a personal computer, where the data analysed using Matlab. At the same time, the medic responsible for supervising the monitoring of the patients, provides the patient's anonymized clinical information. If the signals have quality good enough for research, a complete trustworthy study case has been produced.

Databases and datasets

So far, HGaia's data collection setup has produced just three complete study cases. Therefore, Physionet MIMIC-II (Multiparameter Intelligent Monitoring in Intensive Care) research database [14, 13], was used to obtain physiological signals from several Intensive Care Unit (ICU) patients.

MIMIC database is considered a trustworthy source of data and it is widely used in researches and scientific studies. Its major drawback is that access to patient personal and clinical information is, in most cases, restricted. However, the database provides tens of thousands of records of continuous high-resolution physiological waveforms.

A search for records containing simultaneously intra-arterial BP, ECG and PPG signals, returned hundreds of matches for patients whom age and gender was known. Therefore, two datasets were developed taking into account the characteristics of prototypical users of the system. 28 records of people in their sixties and high average values of blood pressure (at least 135 mmHg) were collected. On the other hand, 25 records of people with less than 40 years old, but showing considerable variations in SBP were also acquired. The records have all a duration of 60 minutes and are close distributed between male and female patients, picked from several times of the day. 13 records, previously studied by Luka Mijatovic, and the 3 study cases from HGaia are added to the 53 specifically gathered records, making up a total of 69 records from 4 different datasets.

1.5 Dissertation structure

This work is organized in four more chapters as follows:

- **Chapter two** provides a sufficient background, and a review of the state of the art, on BP measurement methods, namely the PTT approach, and wearable systems as well. Its objective is to familiarize the reader with the terminology and progresses made so far in these areas, and identify the current trends in development and research.

- **Chapter three** describes and analyses in depth the methods put into use in the study of the models and the results obtained from the experimental setup and optimization techniques applied. Additionally, a system definition is given and modelling is performed to explain real and experimental system requirements, constraints and boundaries utilized; databases used and datasets developed are reported as well.

- **Chapter four** introduces a different approach, a novel application which detects BP events. Motivation, definitions and requirements will first be presented, methodology, detection, evaluation techniques and algorithms will be described after. Finally, results will be provided based on performance graphs and tables.

- **Chapter five** closes this work by putting each section into the wider picture, by identifying which objectives were and were not fulfilled and, ultimately, by providing a set of points representing the outcomes that resulted from the developed work. In addition, future work will be provided through a list of discussion topics representing future strategies on non-invasive blood pressure estimation using a PTT based approach, which may result either from the conclusions drawn or work not performed due to time management options or unavailable resources.

Chapter 2

State of the art

2.1 Methods for measuring blood pressure

2.1.1 Blood pressure characteristics, variability and measurement

Blood Pressure, sometimes referred to as arterial blood pressure, is the force of circulating blood pushing against the walls of blood vessels, named arteries. Each time the heart beats, blood is pumped out into the arteries and distributed all over our body. It constitutes one of the principal vital signs. Systolic blood pressure occurs when the heart is pumping and diastolic blood pressure occurs when the heart is resting [15]. By convention, blood pressure is measured in millimetres of mercury (mm Hg) [16], and is considered normal if it is usually less than or equal to 120/80 mm Hg (120 systolic and 80 diastolic) [17].

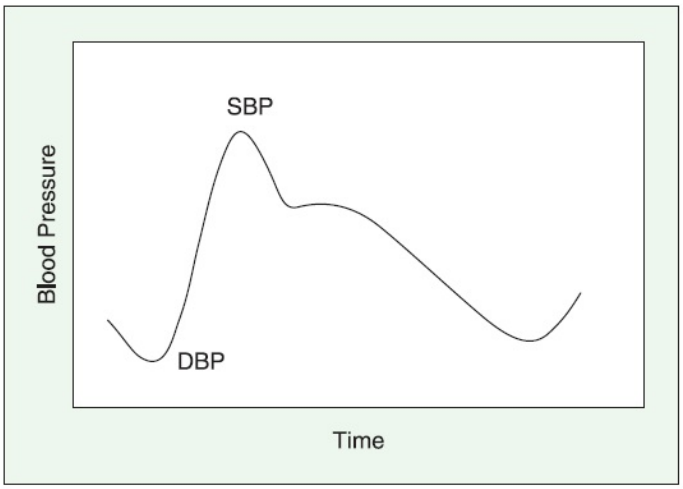

Figure 2.1: Generic **blood pressure waveform** in the arteries (adapted from [18]).

Blood pressure varies throughout the different sites of the human body and suffers spontaneous fluctuations during the day as it is modulated by respiration. There is a considerable range of ways to describe BP variability, from beat-to-beat changes to long-term changes between clinical visits

[4]. Furthermore, it has been showed that biological materials, such as human organs, are more susceptible to damage by changes of pressure rather than steady-state levels and, in consequence BP variability may be considered an independent risk factor for cardiovascular morbidity [19]. Although other studies also point out that BP variability should be considered an important predictor of heart disease development [20, 21], it remains unclear to what extent the pathological effects reported are a manifestation of a damaged organ weakening the baroreflex regulation of BP (which leads to the increase of BP variability) or the direct result of the variability itself [4].

In order to properly analyse this phenomenon, continuous blood pressure recordings with high availability levels are needed [22]. Therefore, a non-invasive continuous blood pressure monitoring system does not only help clinicians to classify patients as normo- or hypertensive but also helps determining the uncertainty and effects introduced by the instability of blood pressure variability.

There are two major approaches when it comes to measuring BP:

1. direct invasive methods;
2. indirect non-invasive methods.

Invasive Methods are generally used in hospitals and intensive care units via the insertion of a catheter into a suitable artery thus providing a "beat-to-beat" record of the patient's BP. This method provides more accurate readings, proving to be very useful in patients that are likely to display sudden BP changes (e.g. vascular surgery), patients that require a close BP control (e.g. head injured patients), or in patients receiving drugs to maintain BP [23]. On the downside, being a method that requires the invasion of the body (skin, tissue and vessel wall) with a hollow needle, its application is limited due to the risks and ethical aspects of the associated invasiveness. Therefore, such measurements usually only take place on seriously ill patients.

Non-Invasive Methods do not require skin penetration but instead the use of a cuff based technique. Although there has been recent developments concerning cuffless measurement systems in a body sensor network (BSN) context, these are not yet available for commercial purposes. Furthermore, indirect measurements provide either a momentary value of blood pressure or a continuous waveform similar to invasive measurements, depending on the technique. Intermittent non-invasive methods, namely auscultation and oscillometry, represent the most common use of blood measurement technology in clinical and ambulatory measurement, respectively. However, all of these techniques have known limitations and do not yet present the same accuracy levels as invasive methods.

2.1.2 Non-invasive blood pressure measurement

According to Ward and Langton [16], intermittent, non-invasive systems are based on three key components:

1. an inflatable cuff;

2. a method which determines the point of systolic and diastolic pressures;

3. a method for measuring pressure.

Mode of Operation: A cuff is placed around a limb, usually the upper arm. It should be approximately 20% wider than the diameter of the part of the limb being used. Smaller cuffs lead to an overestimation of blood pressure and bigger cuffs will lead to an underestimation of blood pressure. The cuff will then be inflated to a pressure above that of the arterial systolic pressure. When this pressure point is reached, the walls of the artery are preventing blood flow. The cuff is then deflated below systolic pressure resuming blood flow. This flow can then be calculated using different resources [16].

Auscultation

This technique was first described by Nicolai Korotkoff in 1905, using the cuff presented by Riva-Rocci in 1896. An inflatable cuff is used to compress the brachial artery and a mercury sphygmomanometer for measuring cuff pressure. Additionally, using a stethoscope it is possible to determine a set of sounds over the brachial artery distal to an upper arm cuff [9]. Four sounds or phases, and later five, were described and its nature attributable to the systolic and diastolic pressures Fig 2.2.

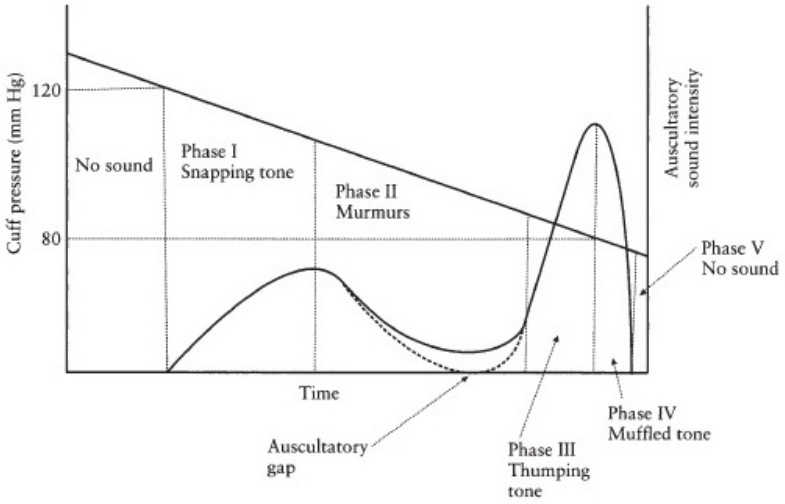

Figure 2.2: Graphical representation of cuff deflation and **sound intensity on auscultation** (adapted from [16]).

In the past, it was debated if the fourth or the fifth Korotkoff sound represents true diastolic pressure. However, there is a current consensus to choose the fourth or the fifth sound which is based on the pulsation audibility when cuff deflation is complete [16]. Although this method constitutes a simple procedure, it requires a trained operator and different interpretations of diastolic pressure may arise and lead to significant variability. The auscultatory method has been the most

frequently applied method for measuring blood pressure but is gradually being replaced by other techniques that are more suited to automated measurement.

Oscillometry

Oscillometry is based on the detection of the oscillations in the cuff pressure during cuff deflation. The technique was discovered by Marey in 1876. The oscillations begin above systolic pressure and continue below diastolic Fig 2.3, so their values can only be estimated using an indirect empirical approach. These effects take place due to the impact of the blood pressure on the cuff and can be seen even for cuff pressure above the systolic blood pressure value, where the arteries under the cuff are closed [18]. It was shown experimentally that the point of maximal oscillation corresponds to the mean intra-arterial pressure [4].

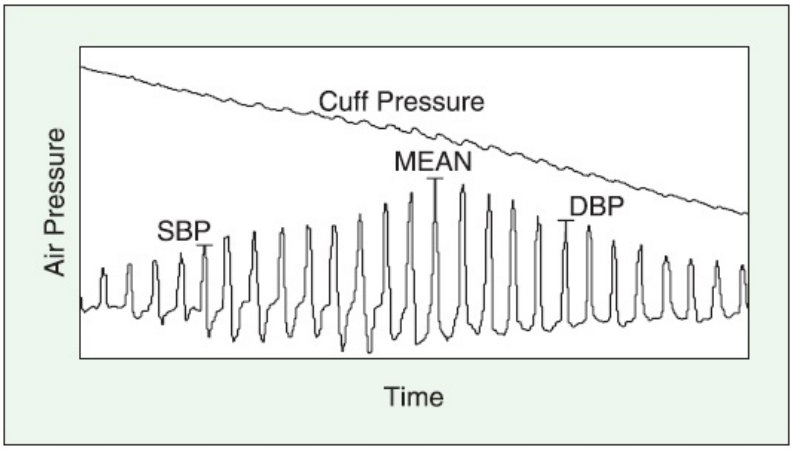

Figure 2.3: **Oscillometry**: The upper curve shows the oscillometric pulses of the cuff pressure. It is depicted the decrease of cuff pressure above systolic blood pressure to below diastolic blood pressure. The lower curve is the upper curve after subtracting the its trend and amplifying the oscillations (adapted from [18]).

As different approximations can be utilized to obtain the systolic and diastolic pressure values, different manufacturers tend to use different criteria. The technique's main advantage is that the cuff doesn't contain sensors which results in its placement not being critical. This leads to patients being able to apply cuffs themselves, making home measurements possible [9]. On the other hand, the amplitude of the oscillations is dependent on other factors, such as the stiffness of arteries, which may lead to underestimation in older people [4]. In addition, the pulsations are easily disturbed by motion artefacts.

Volume-clamp method

This method was introduced by Peñáz in 1973 and is based on the principle of dynamic vascular unloading of the finger arterial walls using an inflatable finger cuff with a built-in photoplethysmographic (PPG) sensor [24].

Plethysmographic devices can't measure blood pressure, but they can measure blood volume changes. Yet, these volume changes can't be transformed into pressure, due to the non-linearity of the elastic components of the arterial wall, as well as the non-elastic parts of the smooth muscles [25]. So, to linearize this phenomenon a counter pressure as high as the pressure inside the artery needs to be applied Fig 2.4. Blood volume can be kept constant if the same pressure is applied from the outside. Therefore, the continuously changing pressure that is needed to keep the arterial volume constant corresponds to the intra-arterial pressure and thus it is an instantaneous, continuous measure for arterial blood pressure [25]. This is the principle behind the vascular unloading technique Fig 2.5.

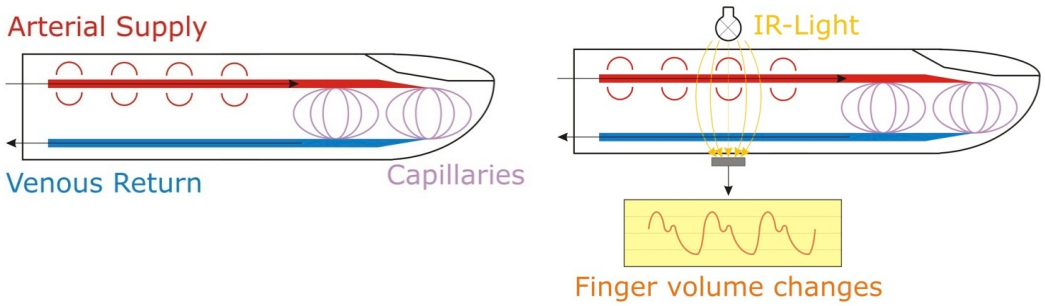

(a) Finger Physiology (b) Plethysmographic method

Figure 2.4: **Plethysmographic method:** Infrared light, emitted from a LED, is sent through the finger. The light is partly absorbed by arterial blood, which changes according to the pulse. A light detector receives the non-absorbed light on the other side of the finger and therefore produces a continuous pulse signal. Figures adapted from *http://www.cnsystems.at/en/vascular-unloading-technique*.

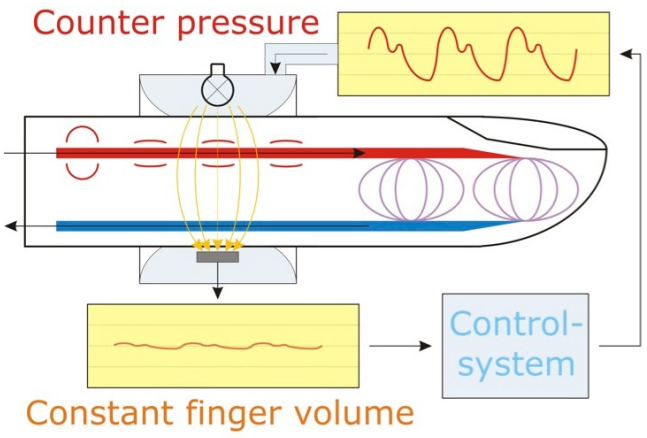

Figure 2.5: **Vascular unloading technique**: The volume signal is fed into the control system that produces a counter pressure in a cuff placed over LED and light detector. The control condition of the system keeps the volume signal constant at any time by controlling the alterable pressure in the cuff (adapted from *http://www.cnsystems.at/en/vascular-unloading-technique*).

Finapres (Finapres Medical Systems, Amsterdam, The Netherlands) technology was introduced in the early 1980s providing the measurement of the arterial blood pressure waveform at the finger on a continuous beat-to-beat basis, using the vascular unloading technique described above Fig 2.5. It uses a extremely rapid servo system with the cuff actuator in order to adjust the pressure in the finger fast enough to keep the photoplethysmograph constant.

Finapres cuff pressure has been compared to intra-arterial pressure in a large number of studies in both awake and anaesthetized subjects. Blood pressure variations were introduced by different means [9]. The obtained wave form using this procedure has been found to resemble to the intra-arterial pressure wave in most subjects and is considered to give an accurate estimation of the changes of systolic and diastolic pressure [4]. Still, results have concluded that the finger arterial mean pressure measured with Finapres is 5 to 10 mmHg lower than intra-arterial pressure in the brachial artery [9]. The Finapres system is no longer commercially available, but alternative blood pressure devices have been introduced: the Portapres and Finometer systems (Finapres Medical Systems BV, Holland) and the Task Force Monitor system (CNSystems Medizintechnik, GmbH) [24].

With the development of the Portapres measurement device it was possible, for the first time, to record long-term 24 h blood pressure profiles and obtain daily variations in blood pressure. In consequence, related cardiovascular parameters of healthy subjects and patients during their normal daily activities could be obtained and analysed [9]. It was considered a breakthrough in ambulatory non-invasive blood pressure measurement.

2.2 The pulse transit time approach to blood pressure measurement

Even though the above described non-invasive methods for measuring BP present good results, their ambulatory characteristics show a number of limitations that makes it unsuitable for individuals to wear in a true comfortable and reliable way. Furthermore, the vertical offset between the measurement location and the level of the heart is often a source of serious measurement error [26].

Potentially the most useful and convenient indirect parameter for achieving a continuous non-invasive measurement of BP in an ambulatory way that is comfortable and reliable is the pulse wave velocity (PWV) or the inverse, pulse transit time (PTT). PTT is the time it takes a pulse wave to travel between two arterial sites, usually from the aortic valve to the finger [5, 15]. The principal factors that determine the speed of propagation of the pulse wave are the stiffness and tension in the arterial walls. In turn, speed propagation of the pulse wave depends to a large extent on blood pressure. An increase in BP means an increase in arterial wall tension and stiffness, thus decreasing PTT, and in reverse a drop in BP decreases arterial wall tension and stiffness, therefore extending PTT [15]. It can then be concluded that PTT is inversely proportional to BP and the falls in blood pressure corresponds to rises in PTT [15].

The theoretical framework behind these statements is known as the Moens-Korteweg equation. It gives us the pulse-wave velocity as a function of vessel and fluid characteristics, thus outlining the relationship between PTT and blood pressure [5, 27]:

$$c = \frac{L}{PTT} = \sqrt{\frac{E.h}{\rho 2R}} \tag{2.1}$$

where c is the wave velocity, L is the length of the vessel, PTT the pulse transit time, ρ is the fluid density, R is the inner radius of the vessel, E is the modulus of wall elasticity (Young's modulus), and h is the vessel thickness. Considering an elastic vessel, there exists an empirical exponential relation between E and the fluid pressure P, in particular:

$$E = E_0 e^{\alpha(P-P_0)} \tag{2.2}$$

where E_0 and P_0 are nominal values of Young's modulus and pressure, respectively, and α is a constant.

There are different ways to measure PTT, such as arterial tonometry, the ultrasound Doppler method or using two aligned PPG sensors located at known distance [5, 28]. However, there is a simpler and more convenient way to measure PPT. It can be computed as the temporal difference between the R wave in an electrocardiogram and the beginning of the following pulse wave measured by photoplethysmography Fig 2.6.

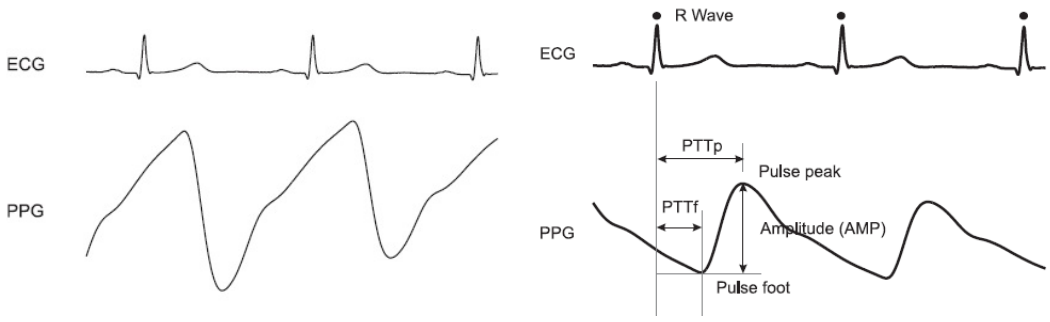

(a) ECG and PPG wave signals

(b) Graphical display of PPT calculation

Figure 2.6: Using pulse wave analysis, the R peak can be identified as well as the PPG pulse peak. Beat-to-beat pulse transit time for both the foot of the pulse (PTTf) and the peak of the pulse (PTTp) can then be computed and the foot-to-peak amplitude (AMP) registered (adapted from [24]).

To find a relation between blood pressure and PPT, equations (2.1) and (2.2) can be used. From those a logarithmic relation between the two parameters is obtained:

$$P = k_1 ln(k_2.PTT) \tag{2.3}$$

where k_1 and k_2 are arbitrary constants and P the fluid pressure, in this case BP. BP can be then estimated using a linearised version of the logarithmic model. Different linearised versions of the

logarithmic model have been used in various cuffless systems that attempt to estimate BP non-invasively, some of which include additional data features, such as heart rate (HR). These models and systems will be explored in the next section.

Concerning the measurement quality of PPT based methods, Marcinkevics [5] indicates several studies that have confirmed the application of PPT for blood pressure measurement and some which implied that PTT was not sufficiently highly correlated to BP in order to indirectly measure it. In addition, he led a study in which he concluded the existence of a close correlation between pulse wave velocity (PWV) and blood pressure. Furthermore, Wong and Zhang [29] conducted and experiment in which the results "implicated that a PTT-based technique could be implemented in a personalized wearable device for non-invasive and continuous monitoring of SBP".

Taking these statements into consideration, it seems beneficial to integrate blood pressure measurement using PTT based models in wearable devices that already perform ECG measurements in a reliable way. This would have a complementary effect, either if the underlying cause is to expand the quantity and quality of services performed, or the fact that ECG measurement may enhance and improve BP estimation results.

2.2.1 PTT based models

Recently, several methods and devices for cuffless BP estimation using PPG signals, have been proposed in the literature. Experiments have been conducted on groups of subjects, where independent instruments are used to acquire ECG and PPG, thus estimating BP. Simultaneously, a reference method for BP measurement is applied and compared with the estimated values. The most frequently used models based on simplified and linearised versions of the Moens-Korteweg equation (2.1) are:

- Cattivelli and Garudadri [27] use models of the form:

$$BP = a \cdot PTT + b \tag{2.4}$$

  which the authors considered to be more robust to noisy measurements.

- Wong and Poon [30] observed that for some cases, BP was highly correlated with instantaneous heart-rate. Furthermore, they considered the arteries to be purely resistive, thus meaning that BP would increase linearly with heart-rate (HR):

$$BP = a \cdot PTT + b \cdot HR + c \tag{2.5}$$

- McCombie *et al* [28] suggested the following model:

$$BP = \frac{a}{PTT^2} + b \tag{2.6}$$

- Lastly, Fung *et al* [31] considered:

$$BP = a \cdot \ln(b \cdot PTT) \tag{2.7}$$

These models have been tested in laboratory conditions and have shown good results between the calculated SBP and DBP values and the ones measured using the reference technique.

On a different perspective, Ferreira Marques *et al* [2] proposed an online calculation of BP based on the method first described by Pandian *et al* [32]:

$$P_{sys} = \left[k_s \times (C_{dx})_i^2\right] + k_{sys\_cal} \tag{2.8}$$

$$P_{dis} = \left[k_d \times (C_{dx})_i^2\right] + \left[k_{IHR} \times IHR_i\right] + k_{dis\_cal} \tag{2.9}$$

where $(C_{dx})_i$ is the inverse of the delay between the R peak of the ECG wave and the 50% slope on the ascending PPG part of the PGG wave of each pulse Fig 2.7.

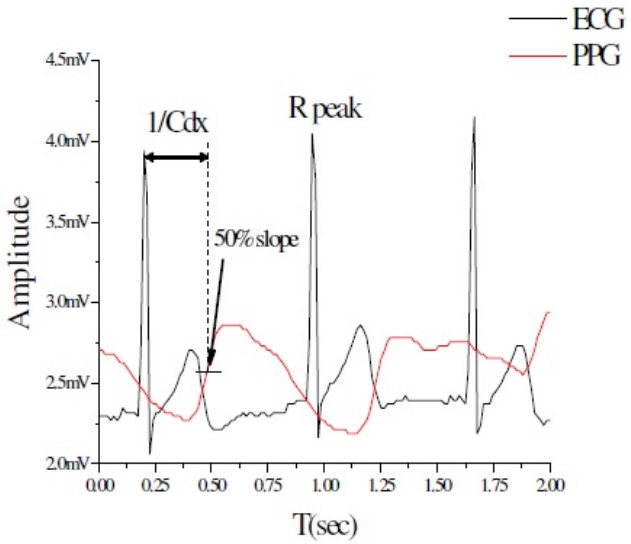

Figure 2.7: Example of PPG and ECG signals with 1/Cdx interval depicted (adapted from [2]).

IHR_i is the instantaneous heart rate for the i_{th} pulse, k_s and k_d are fixed constants; k_{sys_cal} and k_{dia_cal} are the systolic and diastolic calibration constants, k_{IHR} is the constant related to the IHR [2].

2.3 Wearable and ambulatory systems

Wearable devices can combine monitoring, display, treatment and alarming functions. The term "wearable" refers to the feature that the device can be dressed up or used as a form of garment [11]. As stated by Bonato [33], wearable devices provide the opportunity for:

- Monitoring patients for long periods of time;

- Access the daily body condition of the subject at home or outdoor;
- Gather physiological data by using an ambulatory system.

Examples of systems that already perform this type of approach are Sensatex's "Smart Shirt", Vivometrics "Lifeshirt", Zephyr's "BioHarness" and BioDevice's "VitalJacket". These systems measure ECG, heart rate and respiration in a comfortable and reliable way. However, blood pressure measurement does not yet make part of these systems.

2.3.1 Ambulatory blood pressure monitoring (ABPM)

Ambulatory blood pressure monitoring (ABPM) is performed with cuff-based oscillometric devices over a period of about 24 hours. Blood pressure measurements are taken at regular intervals of 20 to 30 minutes during the day, and periods of 1 hour during the night. The device is worn on the belt connected to a standard cuff placed on the arm, and allows the patient to undergo normal daily activities, including sleep, as represented by Fig. 2.8. Its accuracy has been validated in a wide range of patients, provided the correct cuff size. ABPM provides a more reliable measure of a patient's BP than isolated clinic measures, as the patient is less likely to be subject to "white-coat" effect, i.e. BP readings often higher at clinical visits, due to anxiety and stress caused by the clinical settings. Results provide 24 hour, day time and night time BP averages and variability readings.

ABPM devices are considered to be a powerful tool in accurately diagnosing hypertension and providing optimal screening and care. Yet, arterial blood pressure monitoring may be inaccurate in patients with irregular heart rate and arrhythmias and is not designed to detect postural hypotension [10].

Figure 2.8: Arterial blood pressure monitor example (adapted from Farum® S.A. SH-P ABPM device model).

2.3.2 RTAB prototype

The RTAB prototype is an extension of the Vital Jacket® (VJ) ambulatory wearable ECG system. The VJ wearable vital-signs monitor was created by group of researchers at the University of Aveiro in conjunction with a spin-off company named BioDevices S. A. (http://www.biodevices.pt) [2]. It acquires physiological data using textile and microelectronics in a non-intrusive way, taking the form of a simple T-Shirt Fig 2.9.

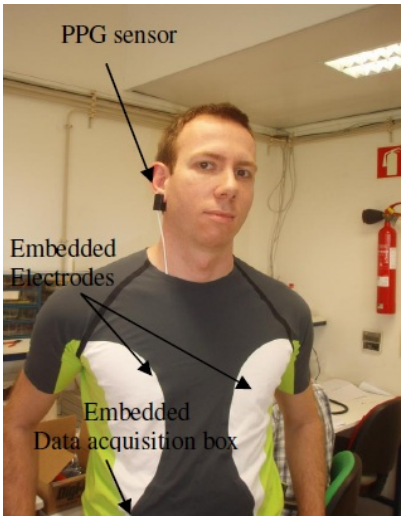

Figure 2.9: Subject wearing an extension of the Vital Jacket®, constituted by ECG electrodes, a PPG sensor located at the right ear and a data logging unit which acquires the physiological signals and stores them(adapted from [12]).

Vital Jacket currently has the EU CE 1011 Medical Device certification clearance, is compliant with the EU directive 42/93/CE and is produced under a ISO9001 and ISO13485 certified manufacturing process [2]. Furthermore, it is already under commercialization and used to perform clinical diagnosis in cardiology and in monitoring high performance sport activities.

Making use of such system's potential, blood pressure estimation is possible by integrating a PPG sensor with the already existing components. This allows the arterial pulse-wave transit time to be measured between the ECG R-wave and the PPG pulse wave. BP can then be estimated using one of the models discussed in 2.2.1. Although PPG measurement sites are available all over the body, the finger, ear or toe have usually been the chosen sites to locate the PPG sensor [24]. This is mainly due to the fact that pulses are easily detected in such sites, but also to the fact that more studies on PPG measurement repeatability and reproducibility have been made from these body sites. Moreover, there are clear differences in pulse characteristics when it comes to the left and right sides of the body, as well as the proximity of the measurement site to the heart [24]. On the other side, PPG sensors located at the referred sites are found to be uncomfortable and unreliable to be used on a daily basis, preventing its user from fulfilling manual tasks in a natural way.

The wrist or forearm have been suggested as a more viable place for locating the PPG sensor in terms of usability. Additionally, it has been suggested the implementation of the sensor in the

form of a watch, communicating with the data acquisition box wirelessly, through radio frequency. This would prove to be a huge step in terms of the system's usability. However, the complete implications of placing the PPG sensor in the wrist or forearm need to be explored as new data is gathered and lab work is conducted, in order to properly understand the effects of choosing this body site to hold the PPG sensor.

Chapter 3

Models for estimating BP using PTT

3.1 Linearised models

As discussed in section 2.2, it is possible to obtain from the Moens-Korteweg equation (2.1), and its logarithm model (2.3), a linearised expression for estimating BP:

$$BP = a \cdot PTT + b \tag{3.1}$$

where a and b represent unknown parameters. Even though this expression has been presented in different ways by several authors, this work focuses on linear models of the form (3.1), as they have been observed to be more robust to noisy measurements [27].

On the other hand, heart rate (HR) has been observed to be strongly related to BP and, as a result it should be taken into account in its calculation [30]. Thus, giving origin to a more complete model, that may be more suitable:

$$SBP = a_1 \cdot PTT + b_1 \cdot HR + c_1 \tag{3.2}$$

$$DBP = a_2 \cdot PTT + b_2 \cdot HR + c_2 \tag{3.3}$$

where $\{a_1, a_2, b_1, b_2, c_1, c_2\}$ are the unknown parameters, which can be interpreted as follows; a and b translate the weight factors of signals PTT and HR in the estimation of BP, respectively, and c represents the average value of BP. This will be referred hereafter as *Model 1*.

This work focuses in the study of SBP because it conveys more medical information than DBP [4].

As PTT can be acquired using three different detection approaches, as seen in Figures 2.6b and 2.7, it is important to explore the effect of the detection on estimation errors.

So, the SBP models under study are the following:

$$SBP_1 = a_1 \cdot PTT_{peak} + b_1, \qquad PTT_{peak}\ only \tag{3.4}$$

$$SBP_2 = a_2 \cdot PTT_{50width} + b_2, \qquad PTT_{50width}\ only \tag{3.5}$$

$$SBP_3 = a_3 \cdot PTT_{foot} + b_3, \qquad PTT_{foot}\ only \tag{3.6}$$

$$SBP_4 = a_4 \cdot HR + b_4, \qquad HR\ only \tag{3.7}$$

$$SBP_5 = a_5 \cdot PTT_{peak} + b_5 \cdot HR + c_1, \qquad Model\ 1,\ PTT_{peak} \tag{3.8}$$

$$SBP_6 = a_6 \cdot PTT_{50width} + b_6 \cdot HR + c_2, \qquad Model\ 1,\ PTT_{50width} \tag{3.9}$$

$$SBP_7 = a_7 \cdot PTT_{foot} + b_7 \cdot HR + c_3. \qquad Model\ 1,\ PTT_{foot} \tag{3.10}$$

AAMI's (Association for the Advancement of Medical Instrumentation) clinical references for blood pressure measurement require that all measurements made using a given technique have error means between $[-5,5]$ mmHg and standard deviations below 8 mmHg, for both SBP and DBP [27, 34]. These will be the values used for reference when analysing the results of each model for a given estimation method.

3.2 Methods for estimating blood pressure using PTT

3.2.1 Least Squares Fitting

Optimization of the models will be performed by applying different methods and algorithms. An obvious first approach would be to determine the calibration constants that minimize the mean squared error (MSE), for each given record. Consider the following definition:

$$MSE = \frac{1}{n}\sum_{i=1}^{n}(\hat{Y}_i - Y_i)^2 \tag{3.11}$$

where $\hat{Y}$ is the estimated SBP vector of n samples and Y is the vector of true values, i.e. invasive SBP. Thus, the MSE measures the average of the squares of the prediction errors, that is the differences between the values predicted by the estimator and the true values of the entity being estimated.

By computing $\hat{Y}$ according to equation (3.2) this will result in:

$$\hat{Y}_{1:N} = X_{1:N}\theta \tag{3.12}$$

where, θ is the 3×1 matrix of unknown constants given by:

$$\theta = \begin{bmatrix} a \\ b \\ c \end{bmatrix} \tag{3.13}$$

and, $X_{1:N}$ is the $N \times 3$ matrix constituted by N observations of PTT and HR from time instants $t = t_1, t_2, \ldots, t_n$:

$$X_{1:N} = \begin{bmatrix} PTT(t_1) & HR(t_1) & 1 \\ PTT(t_2) & HR(t_2) & 1 \\ \vdots & \vdots & \vdots \\ PTT(t_N) & HR(t_N) & 1 \end{bmatrix} \tag{3.14}$$

Therefore, if $Y_{1:N}$ is given by:

$$Y_{1:N} = \begin{bmatrix} SBP(t_1) \\ SBP(t_2) \\ \vdots \\ SBP(t_N) \end{bmatrix} \tag{3.15}$$

the value of θ that minimizes $\|X_{1:N}\theta - Y_{1:N}\|^2$ is [35]:

$$\hat{\theta}_{ideal} = \left[X_{1:N}^T X_{1:N}\right]^{-1} X_{1:N}^T Y_{1:N} \tag{3.16}$$

Provided a $\hat{\theta}_{ideal}$, it will give the "best" constant values of (a,b,c), in the MSE sense, for a given record.

3.2.2 Recursive Least Squares

It is now presented a method that estimates SBP by varying the calibration constants, using a recursive least squares (RLS) algorithm presented by D.S.G Pollock [36]. This approach may be useful to understand how these parameters vary over the time or length of a record. Consider at each instant t the following definition:

$$y_t = x_t \theta_t + \varepsilon_t \tag{3.17}$$

where y_t corresponds to the value of SBP_t, x_t and θ_t are, respectively:

$$x_t = \begin{bmatrix} PTT(t) & HR(t) & 1 \end{bmatrix} \qquad \theta_t = \begin{bmatrix} a_t & b_t & c_t \end{bmatrix}$$

and ε_t is the error term.

To initiate the recursion, an initial estimate θ_0 of θ is needed in conjunction with a corresponding dispersion matrix. $X_{1:tp}$ and $Y_{1:tp}$ matrices are obtained using tp initial observations of SBP, PTT and HR. θ_0 is then obtained using equation (3.16). This phase is known as training period. A dispersion matrix P_0 can then be computed using the following expression:

$$P_0 = \sigma^2 \left(X_{1:tp}^T \cdot X_{1:tp}\right) \tag{3.18}$$

and σ^2 is the sum of the estimated residual variance resulting from calculating b_0:

$$\sigma^2 = \|X_{1:N}\theta_0 - Y_{1:N}\|^2 \tag{3.19}$$

Pollock has presented a summary of the components of the recursive least squares algorithm computed at each iteration. These equations are presented below:

$$h_t = y_t - x_t'\hat{\theta}_{t-1}, \quad \textit{Prediction Error} \tag{3.20}$$
$$f_t = x_t'P_{t-1}x_t + \sigma^2, \quad \textit{Error Dispersion} \tag{3.21}$$
$$\kappa_t = P_{t-1}x_t f_t^{-1}, \quad \textit{Filter Gain} \tag{3.22}$$
$$\hat{\theta}_t = \hat{\theta}_{t-1} + \kappa_t h_t, \quad \textit{Parameter Estimate} \tag{3.23}$$
$$P_t = (I - \kappa_t x_t)P_{t-1}. \quad \textit{Estimate Dispersion} \tag{3.24}$$

3.2.3 Exponentially-Weighted regression

The Exponentially-Weighted regression (EWR) algorithm is an extension of the RLS algorithm. As the number of observations grows, a greater weight may be given to more recent data, rather than to data that has reached a certain age. Also, discarding observations that have passed its date of expiry is a relevant procedure when the processes that generate the data are subject to sudden structural changes. As a result, the algorithm ensures that any false or inaccurate information within the data that predates a structural change will not be memorized permanently. So, an exponential weighting arrangement applied to the data may serve this purpose [36].

Let $\lambda \in]0,1]$ be the rate at which the data is discounted, then the EWR algorithm will be constituted by equations (3.20), (3.22) and (3.23), plus equations (3.21) and (3.24), containing λ, the *forgetting factor*, which will be re-written below:

$$f_t = x_t'P_{t-1}x_t + \lambda\sigma^2, \quad \textit{Error Dispersion} \tag{3.25}$$
$$P_t = \lambda^{-1}(I - \kappa_t x_t)P_{t-1}. \quad \textit{Estimate Dispersion} \tag{3.26}$$

3.2.4 Increasing the time period between iterations

Each time that an iteration of the RLS or EWR algorithm is performed, an observation of SBP is "consumed", in other words, a true value of SBP is needed every time an update of θ should be performed to better predict the changes that may occur in SBP for a variety of factors.

However, in a real environment true values of SBP are not available by invasive monitoring but only through non-invasive measurements performed by, namely, home BP cuff monitors. Thus, true SBP values are not available on a heartbeat basis but at a minimum rate of about 1 minute, which is approximately the duration of a home BP monitor measurement.

The procedure described below is based on previous methods and takes these real environment constraints into account.

Consider tp initial observations of SBP, obtained using a home BP monitor, PTT and HR. Then, in the conditions expressed in 3.2.1, through equations (3.11) to (3.16), a θ_0 will be obtained

based on the initial observations. It has been observed by Cattivelli and Garudadri [27] that tp is usually between 10 and 40 measurements of SBP. Obtained a θ_0, the EWR algorithm is applied by iterating every T minutes, at a cost of a new SBP measure taken using the home BP monitor. During the time between iterations, SBP is estimated according to the chosen model, (3.4) through (3.10), based on the observations of PTT and/or HR during that period, and using $\theta = \theta_{nT}$, where θ_{nT} is the value of θ at the n^{th} iteration of EWR with period T. T will be named hereafter as calibration period.

3.3 Results

In this section, the methods described previously are applied to 69 records of 4 different datasets.

First, θ_{ideal} for each record is determined through LSF, and SBP consequently estimated, using the models provided in 3.1. Then, the parameters of the models that produce lowest estimation errors (error mean, error standard deviation and minimum squared error), are analysed in search for some relation with the mean value of SBP. The objective is to study these signals off-line, i.e. having access to all of the true values of SBP, in order to try to obtain concrete information, specifically parameter information, on their behaviour.

Secondly, RLS and EWR are applied in the same conditions as the LSF method: off-line and for the same models. The objective here is to study how θ evolves throughout the records duration, and if it can be found a relation between better, or worse, performance cases and parameter variation. Also, explore if any characteristics in those cases can be linked to the ones obtained by LSF.

Lastly, the results of applying EWR with different iteration periods T are discussed. This is the procedure that replicates better how the on-line ambulatory non-invasive BP measurement device would operate. The process will be reviewed and its performance analysed by looking at estimation errors for the various values of T and by looking at θ and parameter variability. Possible enhancements and future directions may be suggested based on evidence.

3.3.1 LSF method results

Table 3.1 summarizes the estimation errors obtained from applying LSF off-line, for the 7 models defined in 3.1. The results confirm that models which use PTT and HR together in SBP estimation, carry in fact more information than models based on PTT or HR alone. This is in accordance with Wong and Poon (2009) [30].

Furthermore, for Model 1 – PTT_{peak}, 17 of the 69 records did not meet AAMI's requirement for less than 5 mmHg of error mean, and 11 for less than 8 mmHg of error standard deviation. This may suggest that for some specific patients or particular situations, this model does not lead to acceptable BP measurements. However, as no more data is available concerning patient's medical details and external factors at the time of invasive BP recordings, no strong assumptions can be secured, and therefore no concrete conclusions can be made towards bad performance cases. Yet, for most of the cases, there seems to be enough information available in the signals, if the

	Least Squares Fitting (LSF)		
Model	**Mean** (mmHg)	**St.D.** (mmHg)	**MSE** (mmHg^2)
PTT_{peak} only	4.29	5.49	40.82
$PTT_{50width}$ only	$-^*$	–	–
PTT_{foot} only	4.42	5.59	41.82
HR only	4.69	5.95	51.70
Model1, PTT_{peak}	3.82	4.92	33.43
Model1, $PTT_{50width}$	–	–	–
Model1, PTT_{foot}	3.90	4.99	33.56

Table 3.1: Error mean, error standard deviation(St.D.) and minimum squared error (MSE) for the different models, averaged over all records, using the Least Squares Fitting method described in 3.2.1. * – It was not possible to compute $PTT_{50width}$ using the detection toolbox available.

parameters are correctly accounted for, to carry a clinically acceptable SBP measurement. These parameters will now be studied in more depth.

Figure 3.1 depicts the 52 (a,b) pairs, obtained from Model 1 – PTT_{peak} and Model 1 – PTT_{foot}, for records that met AAMI's requirements. There seems to be no strong relationship between the values a and b. The mean and standard deviation for the values of a and b are respectively $a_{mean} = -171.7$, $a_{std} = 370.3$, $b_{mean} = -15.4$ and $b_{std} = 113.6$. Except for a few cases, in peak detection, a seems to be dominant on the negative abscissa and between values $[-1000, 500]$. On the other side, b takes equal weight on positive and negative ordinate and between values $[-250, 250]$.

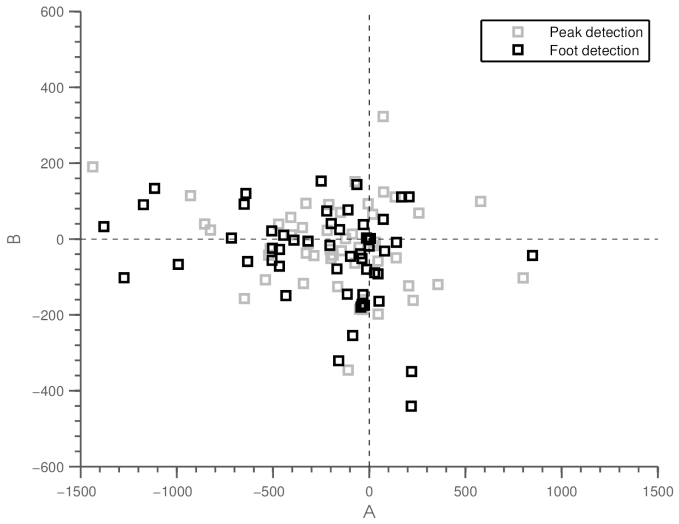

Figure 3.1: Distribution of a,b pairs obtained from calculating θ_{ideal} by LSF.

There is no relationship between the cases where the values of a or b are outside this scope, and bad performance cases, i.e. cases where estimation errors do not meet the clinical requirements. The same goes for pairs with positive values of a. This is confirmed by calculating the correlation coefficients between the values of a and b for all the records, just for the ones that met AAMI's requirements and just for the ones that did not: $\rho_{all} = -0.150$, $\rho_{accepted} = -0.190$ and $\rho_{rejected} = -0.145$, respectively.

However, it has been observed in some cases that a minimum MSE approach does not provide the best resemblance of SBP curve shape, which may be more important if the goal is to monitor variability instead of mean BP level. A future direction, would be to design and implement a technique that would measure this effect more systematically and accurately, and would help understand better the relation between the shapes of the invasive and estimated SBP curves, as demonstrated by Fig. 3.2.

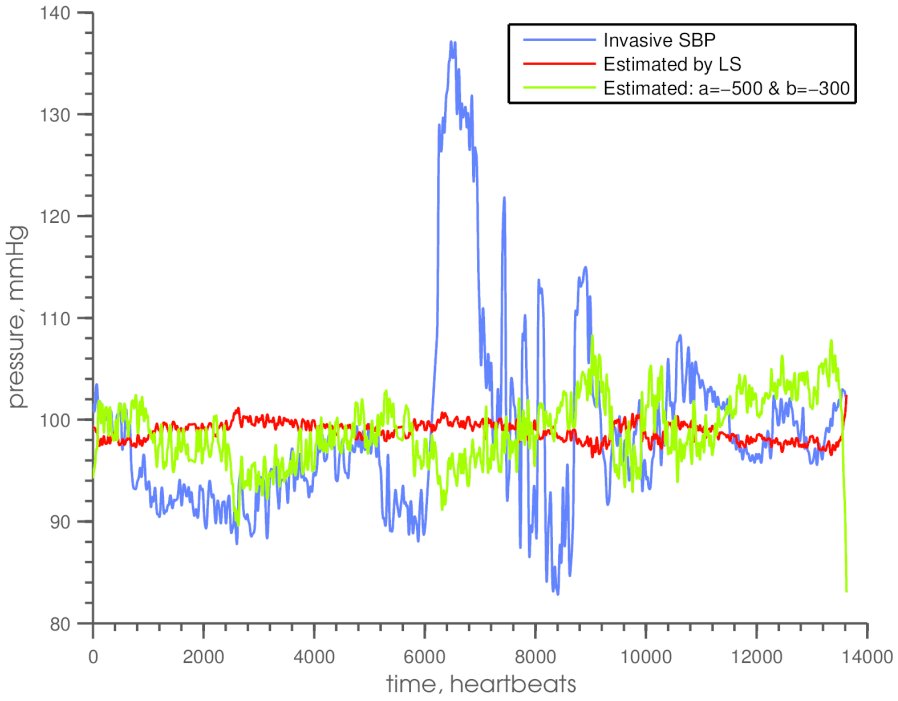

Figure 3.2: Red and green curves represent estimated SBP by LSF and by fixing a and b at specific values, respectively. c is equal in both cases. MSE(LSF) = 87.5 and MSE(FIXED) = 104.5, illustrating that lower MSE does not imply better curve resemblance.

3.3.2 RLS and EWR methods results

Table 3.2 and 3.3 characterizes the estimation errors when applying RLS and EWR off-line, for the 7 models provided in 3.1. Even though RLS performs slightly worse than LSF, EWR's estimation errors indicate that it is possible to track the signal if there is enough physical information available.

Although EWR gives the lowest estimation errors, iterations on recursive algorithms are performed on a heartbeat basis, which is possible only when there is access to the invasive SBP signal, for they require real observations of SBP to iterate. Therefore, these methods can not be applied in a real non-invasive ambulatory BP measurement system, but they provide some information on how the unknown parameters evolve during the course of the record.

To illustrate the time evolution of the parameters, the 10 records of maximum duration, each with length 2 hours and 13 minutes, were studied by analysing how parameters a and b evolve in time using RLS in comparison to a_{ideal} and b_{ideal}, obtained from θ_{ideal} by LSF.

	Recursive Least Squares (RLS)		
Model	**Mean** (mmHg)	**St.D.** (mmHg)	**MSE** (mmHg^2)
PTT_{peak} only	4.70	5.18	50.02
$PTT_{50width}$ only	–*	–	–
PTT_{foot} only	4.66	5.16	49.08
HR only	4.92	5.49	58.88
Model1, PTT_{peak}	4.28	4.88	42.75
Model1, $PTT_{50width}$	–	–	–
Model1, PTT_{foot}	4.21	4.88	41.13

Table 3.2: Error mean, error standard deviation(St.D.) and minimum squared error (MSE) for the different models, averaged over all records, using the Recursive Least Squares method described in 3.2.2. It was used $tp = 150$, for the measures of SBP in the first 150 heartbeats.
* – It was not possible to compute $PTT_{50width}$ using the detection toolbox available.

	Exponentially-Weighted Regression (EWR)		
Model	**Mean** (mmHg)	**St.D.** (mmHg)	**MSE** (mmHg^2)
PTT_{peak} only	0.70	1.00	1.20
$PTT_{50width}$ only	–*	–	–
PTT_{foot} only	0.71	1.04	1.33
HR only	0.74	1.10	1.44
Model1, PTT_{peak}	0.53	0.80	0.77
Model1, $PTT_{50width}$	–	–	–
Model1, PTT_{foot}	0.54	0.81	0.80

Table 3.3: Error mean, error standard deviation(St.D.) and minimum squared error (MSE) for the different models, averaged over all records, using the Exponentially-Weighted regression method described in 3.2.3.
* – It was not possible to compute $PTT_{50width}$ using the detection toolbox available.

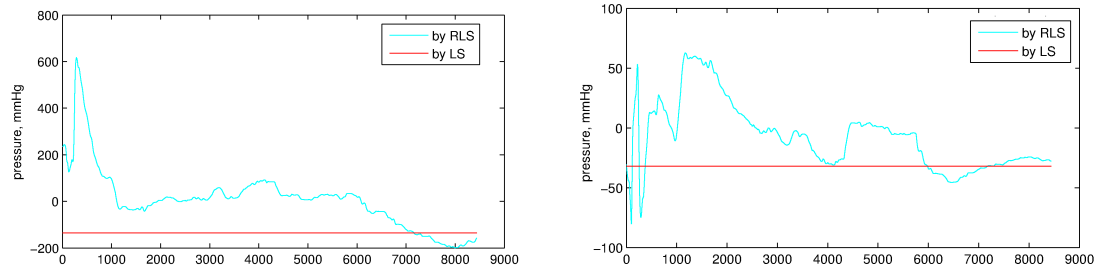

(a) Parameter a evolution and ideal value for record $R1$

(b) Parameter b evolution and ideal value for record $R1$

Figure 3.3: Parameters a and b evolution by RLS, in light green, versus its ideal match by LSF, in red, for a 2 hours and 13 min duration record. Example of a case where RLS evolution value tends to the value of the ideal parameter, calculated by LSF.

Graphical analysis indicate that in about half of the 10 cases that a and b RLS parameters tend, in the end of the record, to their respective LSF value. In the other half, this is not observed, as exemplified in figures 3.3 and 3.4. Furthermore, neither seems to be a link between larger MSE cases and the tendency just described nor the evolution of the parameters show any systematic components.

The interpretation that can be made here is that the model is too simple to take into account

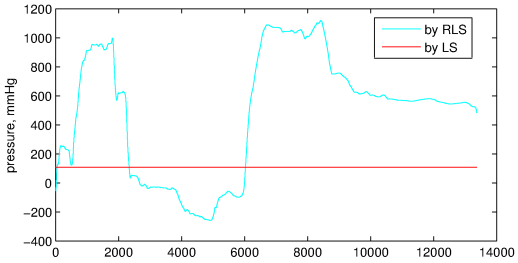

(a) Parameter a evolution and ideal value for record $R2$.

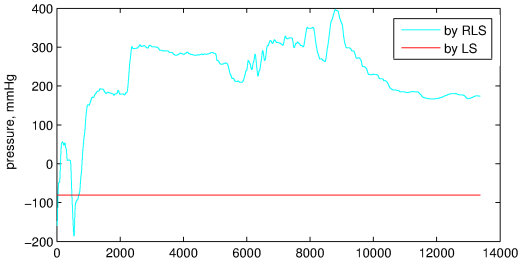

(b) Parameter b evolution and ideal value for record $R2$.

Figure 3.4: Parameters a and b evolution by RLS, in light green, versus its ideal match by LSF, in red, for a 2 hours and 13 min duration record. Example of a case where RLS evolution value does not tend to the value of the ideal parameter, calculated by LSF.

all the factors that can influence and cause variations in BP. Therefore, parameters a and b hold too little physical information, to be able to predict accurately changes in BP that are translated in large variations of their values.

3.3.3 EWR with increasing calibration periods results

Reviewing the method first presented in 3.2.4, an initial calibration operation is performed using 40 measures of SBP, PTT and HR, taken every 15 seconds, from the first 5 minutes of the invasive SBP, PTT and HR signals, yielding $\theta_0 = [a_0 \;\; b_0 \;\; c_0]^T$. SBP is then estimated from Model 1 – PTT_{peak} and θ_0, from minute 5 until instant $5+T$ is reached. At this point in time, EWR algorithm is applied, performing an iteration which uses an observation of invasive SBP, thus re-calibrating the system by re-calculating θ. The new value of θ is then applied to Model 1 to calculate SBP during the period of time $]5+T,\; 5+2T]$. These operations are performed until the duration of the record is reached or $5+2T$ exceeds it. Therefore, the number of iterations performed, n, depends directly on T, and $nT <$ duration of the signal $-$ time of initial calibration $(5$ minutes$)$. The *forgetting factor* used in this procedure was $\lambda = 0.95$.

As 59 of the 69 records have a duration of approximately one hour, the algorithm will be applied using the following values of $T = \{1, 5, 15, 30, \infty\}$ minutes, where $T = \infty$ represents the case where only initial calibration is performed, without conducting further re-calibrations.

	EWR with period T – Estimation errors		
Calibration period	**Mean** (mmHg)	**St.D.** (mmHg)	**MSE** (mmHg^2)
$T = 1$ *min*	-0.17	4.63	36.94
$T = 5$ *min*	-0.51	6.76	105.65
$T = 15$ *min*	-0.48	7.96	163.81
$T = 30$ *min*	-0.77	8.68	228.23
$T = \infty$	-1.48	9.96	373.64

Table 3.4: Estimation errors for Model 1 – PTT_{peak}, averaged over all records, applying the EWR algorithm with different periods of calibration T, as described in 3.2.4. $T = \infty$ denotes that no re-calibration is performed after the initial calibration.

Applying this method to Model 1, PTT_{peak}, table 3.4 represents the estimation errors for the several values of T. It is possible to observe that the standard deviation of the error and MSE increase considerably with T. This fact strongly suggests that θ_0 becomes increasingly obsolete within an hour or half an hour.

	EWR with period T - Parameters			
Calibration period	**Mean(a)**	**Std(a)**	**Mean(b)**	**Std(b)**
$T = 1$ *min*	-206.87	252.49	-26.66	88.70
$T = 5$ *min*	-229.95	260.41	-46.79	95.06
$T = 15$ *min*	-178.25	263.23	-47.00	90.91
$T = 30$ *min*	-144.33	300.74	-28.00	83.69
$T = \infty$	-283.46	0.00	-46.99	0.00

Table 3.5: Mean and standard deviation of the unknown parameters calculated initially and re-calculated at every point of calibration, i.e. nT, where n is the n^{th} iteration of the algorithm and T is the calibration period. $T = \infty$ denotes that no re-calibration is performed after the initial calibration.

On the other hand, this may be due to a lack of robustness of the algorithm hinted by the results depicted in Table 3.5. More specifically, table 3.5 shows a large variability of parameters a and b, between calibrations, which can be a result of very noisy measurements of SBP, PTT and HR. In turn, this means that parameters a and b should be kept within certain limits, by developing a mechanism for enhancing robustness, as done by Cattivelli and Garudadri (2009) [27].

Chapter 4

BP event detector (BED)

4.1 Motivation for BED

The results of the previous chapter, 3.3, indicate that Model 1 – PTT_{peak}, (3.8), is probably not suitable for continuous ambulatory BP estimation without periodic re-calibrations of 30 to 60 minutes. Although, due to time constraints, no particular method was developed to measure this more objectively, partial to full similarity was graphically observed in many cases. Thus, the question whether the model can predict BP variability, particularly important structural changes, that is variations of considerable magnitude, needs to be addressed. In other words, if an external or internal factor, or combination of those, causes a patient's BP to rise or fall to a value, or at a rate that may be considered dangerous, can this model account for it?

In order to address this question, it was considered of relevance to design a system that is able to detect blood pressure events based on large BP variations. Clinical references at HGaia were consulted to determine what constitutes a blood pressure event, and the criteria to classify an event as important and of significance. Two requirements were seen fit as to represent a BP event:

1. **Requirement one –** There is a clear tendency of the mean value of SBP to increase or decrease within the last 30 or less minutes. Two distinct examples are: one, a slower, progressive shift of SBP mean from a higher value to a lower one, or vice-versa, in approximately 30 minutes. Two, a sudden fall or raise of SBP levels, that is, in less or between 5 to 10 minutes, not accompanied by a recovery of the signal to match its prior state or mean level.

2. **Requirement two –** The variation described in item one, is of amplitude 20 mmHg or higher.

Two applications of a BP event detector were identified as useful and promising by medical connections at HGaia. Firstly, an application which is able to detect BP events correctly and reliably from a SBP invasive curve could serve as a helping tool for nurses or doctors in an intensive care unit (ICU), or nursing room, where the patient's BP is being monitored invasively. This would allow the medical staff to engage in parallel activities, knowing beforehand that if some event that

requires medical attention and relates to a BP event would be triggered in a patient, the monitor would release an alarm. This would allow them to use their time more efficiently.

Secondly, a device that non-invasively estimates SBP, detects events from its curve and can be used in an ambulatory manner, independently or in complement with other BP measurement cuff-devices for home use, would prove of great usefulness, as nothing of the sort is available in the market. Although invasive and estimated BP curves might be similar in shape, there will be differences that may prove significant in some cases, resulting in false or missed positive detections. This is the device of interest in this work and which will be object of study.

Therefore, in order to evaluate the performance of the desired device in respect to sensibility and specificity, ROC curves need to be developed. For that matter, a ground truth (GT) needs to be established. A dataset of invasive SBP curves with BP events marked in agreement by three different doctors, should be used as reference to create the GT. As such dataset was not available in time to be included in this work, the BP events were selected by applying the event detection algorithm on invasive SBP signals 1.4.

The steps that comprise the BP event detection approach are analysed in more detail below.

4.2 Event detection approach

4.2.1 ROC analysis and classifiers

As described by Tom Fawcett in *An introduction to ROC analysis* [37], ROC graphic analysis is a technique of visualization, organization and selection of classifiers based on their performance. It has been widely used in signal detection theory and diagnostic systems, as it allows the representation of tradeoff between hit and false alarm rates of classification models.

The performance of classification problems is usually measured using a two-class classifier approach. Consider a classification problem where each instance I is mapped to one element of the set {**pos**,**neg**} of positive and negative class labels.

Given an instance, the classifier outputs an instance as $\{p,n\}$, which results in one of four possible situations. If the instance is positive and is classified as positive, it is considered a *true positive*; otherwise, if it is classified as negative, it counts as a *false negative*. On the other hand, if the instance is negative and is classified as negative, it is considered a *true negative*; otherwise if it is classified as positive, it counts as a *false positive*. Given a test data set (set of instances), the outputs of the classifier can be organized and summarized in a two-by-two *confusion matrix*, as shown in Fig. 4.1. The values along the main diagonal represent the correct decisions made, and the minor diagonal represent the errors made. In the field of statistical hypothesis testing, these are referred to Type I and Type II errors. Type I errors correspond to false positive errors, that is, instances being classified as positive when they are negative. Type II errors correspond to false negative errors, that is, instances being classified as negatives when they are positive [38].

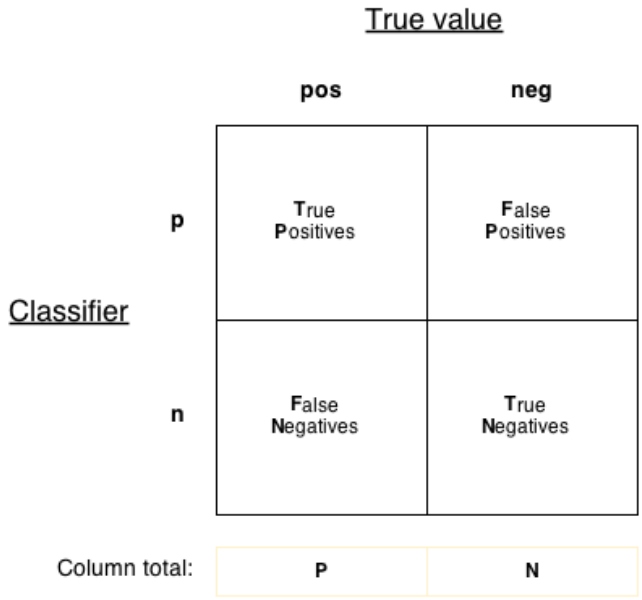

Figure 4.1: Confusion matrix used in two-class classification problems.

Common performance metrics usually calculated from the confusion matrix are presented below [37]:

$$\text{True positive rate} \approx \frac{\text{True Positives}}{\text{Total Positives}} = \frac{TP}{P} \tag{4.1}$$

$$\text{False positive rate} \approx \frac{\text{False Positives}}{\text{Total Negatives}} = \frac{FP}{N} \tag{4.2}$$

$$\text{Sensitivity} = \text{recall} = \text{tp rate} \tag{4.3}$$

$$\text{Specificity} = \frac{\text{True Negatives}}{\text{False Positives} + \text{True Negatives}} = \frac{TN}{FP+TN} = 1 - fprate \tag{4.4}$$

$$\text{Accuracy} = \frac{\text{TP}+\text{TN}}{\text{P}+\text{N}} \tag{4.5}$$

$$\text{Precision} = \frac{\text{TP}}{\text{TP}+\text{FP}} \tag{4.6}$$

ROC space is defined by true positive and false positive rates (TPR and FPR) as X and Y axis respectively. A ROC graph depicts the relative tradeoff between benefits (true positives) and costs (false positives). As TPR equals to sensitivity and FPR equals to $1-$ specificity, the ROC graph is also called the sensitivity vs $1-$ specificity plot. Fig. 4.2 represents a ROC graph with five discrete classifiers labeled A through E. A discrete classifier outputs only a class label, thus producing a (fp rate, tp rate) pair which corresponds to a single point in ROC space [37].

Analysing ROC space and the meaning of a given point's location in it, there are several points of interest to note. The lower left point (0,0) represents the case of never issuing a positive

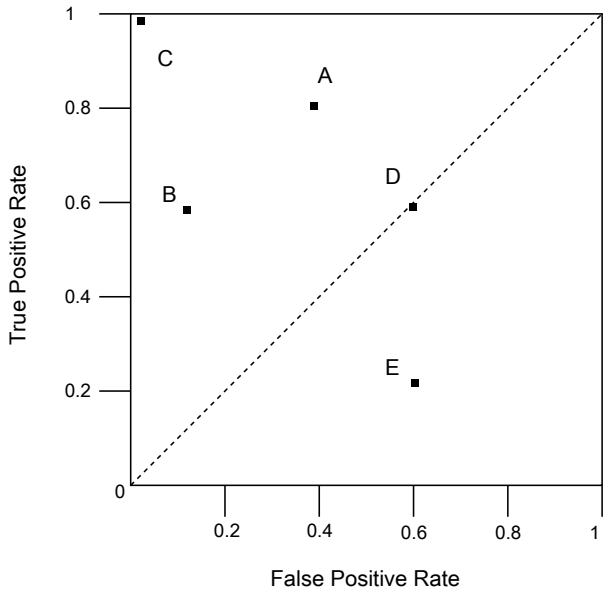

Figure 4.2: ROC space and example of five discrete classifiers.

classification; no false positive errors are committed but no true positives are gained either. On the contrary, always issuing positive classifications is represented by the upper right point (1,1). Perfect classification, that is, always issuing true positives and never false positives, is represented by point (0,1). Classifier C's performance is nearly perfect as seen in Fig. 4.2.

Informally, it is considered that one point's performance is better if localized to the northwest of another. Points localized closer to the X axis, on the left side of a ROC graph, are considered "conservative", as they make positive classifications with solid evidence, thus making few false positive erros, but often having low true positives rates in return. On the other hand, classifiers closer to the upper right side of a ROC graph, are considered "liberal", as they make positive classifications with poor evidence, thus classifying nearly all positives correctly, but having an undesired high false positive rate in return [37]. Hence, classifier B is considered to be more conservative than A, and A is considered to be more liberal than B.

Points in the diagonal $y = x$ represent random classifiers. Point D (0.6,0.6) is a random classifier. It guesses the positive class about 60% of the time, thus is expected to get 60% of positives correct but its false positive rate will increase to 60% as well.

Classifiers located under the main diagonal perform worse than random classifiers. This lower right triangle is usually empty in ROC graphs, because any classifier placed there can be negated to produce a point on the upper left triangle.

4.2.2 Steps in a BED sequence

Table 4.1 reproduces the main steps taken in a BP event detection sequence.

Step 1 computes the PTT and HR signals from the ECG and PPG physiological data files. The invasive SBP signal is also extracted to be used in the formation of the ground truth. Function *GetSinais()* represents this operation, receiving a string as an input, the name of a specific dataset or a empty string specifying every dataset available; it also receives the type of PTT detection: peak, 50% slope or foot. It returns a struct array, for all records, with the fields *PTT*, *SBP*, *HR* and *time*, representing the signals mentioned above, plus the duration of the record.

Step 2 comprises the formation of the Ground Truth. This is done by segmenting the SBP invasive signal and subsequently by applying a specific algorithm for SBP event detection. Function *signalSegmentation()* receives a given signal as input and segments it into n pieces, where $n = 2^p$ and p is chosen between 1 and p_{max}, which is the second input parameter; the result is an array of size n with the segmented signal. Function *eventDetection()* takes the resulting vector and searches for events based on the value of the segments, returning a binary vector of the same size as the input vector, representing the occurrence of an event or not in each segment. These operations will be described in detail in the following two subsections.

Step	**Description**	**Tier 1** functions used	**Tier 2** functions used
1	Extract physiological signals (SBP, PTT, HR, DBP) from data files.	*GetSinais()*	*PrepareDataset()* *GetABP()* *GetPTT()* *GetIHR()*
2	Establish Ground Truth.	*groundTruth()*	*signalSegmentation()* *eventDetection()* *countEvents()*
3	Determine estimated SBP in respect to step 1.	*lsFitting()* or *realEWR()*	
4	Detection of events from estimated SBP.	*estimatedDetection()*	*signalSegmentation()* *eventDetection()* *countEvents()*
5	Compare GT from step 2 and events detected from step 4. Calculate performance metrics.	*compareEvents()*	*processEvents()*
6	Generate a ROC curve by applying steps 4 and 5 repeatedly for decreasing threshold values.	*generateRoc()*	

Table 4.1: Main steps in a BP event detection sequence.

Step 3 proceeds to estimate SBP of all input records, based on acquired signals at step 1. Model 1 – PTT_{peak} is either applied by method LSF or EWT with calibration period T(3.2.1 and 3.2.4) on estimation of SBP. Functions *lsFitting()* and *realEWR()* represent the two processes, respectively.

Step 4 searches for events in the estimated SBP signals computed in step 3. Analogously to step 2, this is done by applying functions *signalSegmentation()* and *eventDetection()*. The main difference lies on the input signal, which is the estimated SBP signal instead of the invasive one.

Step 5 takes the outputs of step 2 and 4 and processes them for subsequent comparison. In other words, processing enables the elimination of possible phase discrepancies and multiple flaggings of the same event. This is accomplished by calling function *processEvents()*. Comparison of processed GT and estimated events is done by function *compareEvents()*. It counts the number of positive and negative detections, as well as true and false positives, and true and false negatives of the estimated events in respect to the GT. Finally, it computes the sensitivity and specificity, among other performance metrics, and the respective point in ROC space.

Step 6 finalizes the BED sequence by generating a ROC curve for the GT generated from the input data files, using a given way of acquiring PTT, and a model and method for estimating BP. This operation is performed by function *generateROC()*, which performs steps 4 and 5 repeatedly for threshold values varying from ∞ to 0, thus generating ROC points increasing by $false\ positive\ rate$.

4.2.3 Signal segmentation

On Stoffer's Fourier-Walsh analysis of time series and statistical theory, David R. Brillinger's commented on a simple technique to examine time series data for level changes [39].

Consider a continuous signal sampled at a frequency of F_s, thus its discrete representation being constituted by *size* samples. Now consider that the signal is broken into n ideally equal parts, which will be called segments, where $n = 2^p$ and $p = 1,2,3,4,p_{max}$; and p_{max} is usually equal to 4 or 5. The signal, after segmentation, will be composed by n segments, numbered from 1 to n. Each segment will be evaluated as the mean value of the samples that are comprised in that segment, that is, for a given i^{th} segment, its value will be computed by $\frac{1}{m}\sum_{j=m_i}^{m_{i+1}} x_j$, where $m = \lfloor \frac{size}{n} \rfloor$, $m_i = [m \times (i-1)] + 1$ and $m_{i+1} = m \times i$. An exception occurs in the last segment if the remainder of $\frac{size}{n}$ is different than zero. The last segment, lets say i_n, is then computed by $\frac{1}{m}\sum_{j=m_n}^{size} x_j$, where $m = \lfloor \frac{size}{n} \rfloor + R$, in which R is the residue of $\frac{size}{n}$, and $m_n = \lfloor \frac{size}{n} \rfloor \times (i_n - 1)$.

In Fig. 4.3 is depicted the graphic output of an example of the process described above for a segmentation of an invasive SBP signal, using $p_{max} = 4$.

The purpose of applying this technique is to be able to represent the signal in a way that makes it easier to detect structural changes, but still remain faithful to its morphology. From the various representations of the original signal, obtained from varying $p = 1$ until $p = p_{max}$, one value of p represents best the signal and its structure. It is now presented an automatic method for finding the best representation, based on the Akaike Information Criterion (AIC).

The Akaike Information Criterion was first presented in 1974 by Hirotugu Akaike, as a novel look at statistical model identification [40]. It is still widely used today, as it provides a way for

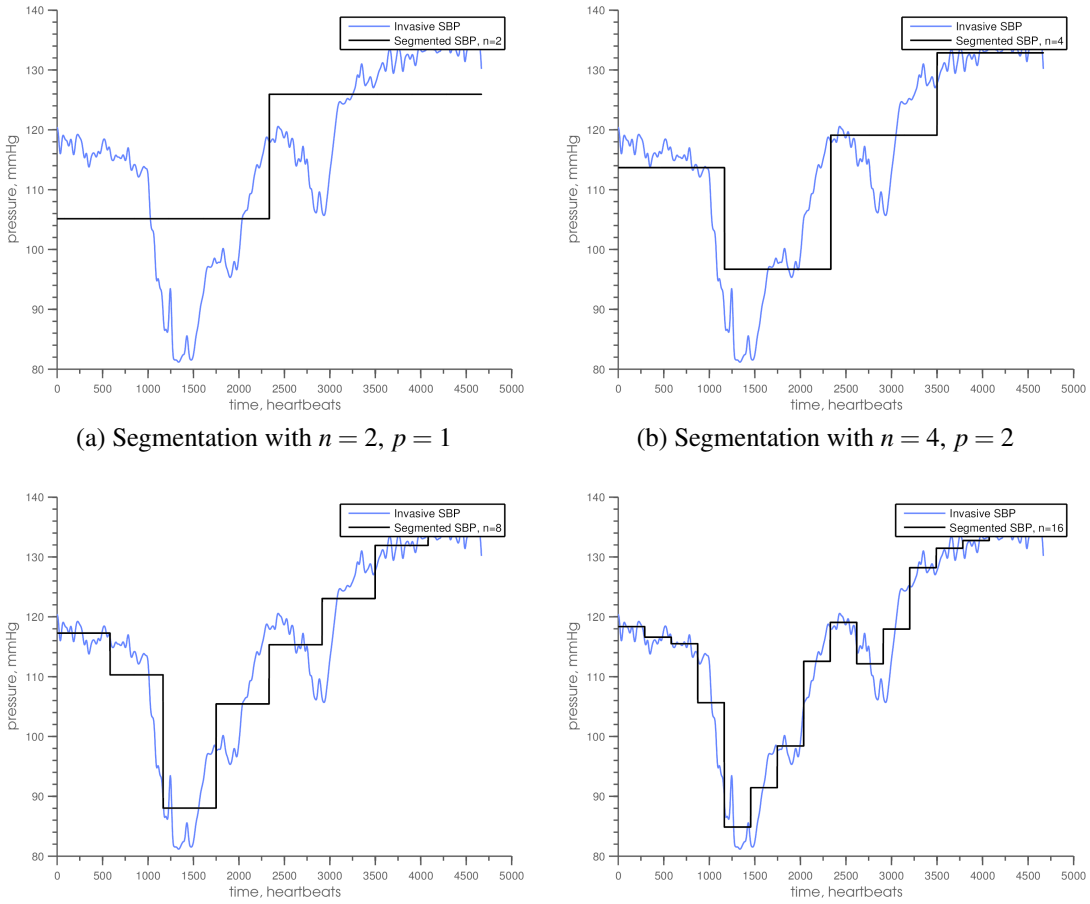

(a) Segmentation with $n = 2$, $p = 1$

(b) Segmentation with $n = 4$, $p = 2$

(c) Segmentation with $n = 8$, $p = 3$

(d) Segmentation with $n = 16$, $p = 4$

Figure 4.3: Example of different segmentation processes (in black) obtained from an invasive SBP signal(in blue), by varying p from 1 to $p_{max} = 4$.

model selection by measuring the relative quality of a statistical model, for a given set of data. It proposes a relative estimate of the information lost when a given model is used to represent the process that generates data.

In a regression context, the one adopted in this work, Shumway and Stoffer [41] suggest the following definition:

$$AIC = \ln \hat{\sigma}_k^2 + \frac{n+2k}{n}, \tag{4.7}$$

where k is the number of parameters in the model, and $\hat{\sigma}_k^2$ is given by equation (4.8).

$$\hat{\sigma}_k^2 = \frac{RSS_k}{n}, \tag{4.8}$$

where RSS_k designates the residual sum of squares under the model with k regression coefficients. For $k = 0$, it corresponds to the sum of squared deviations from the mean:

$$RSS_0 = \sum_{t=1}^{n} (x_t - \bar{x})^2 \tag{4.9}$$

For this particular statistical model AIC equation (4.7) can be re-written as equation (4.10).

$$AIC = \ln\left(\sum_{i=1}^{n}\sum_{j=1}^{k}(x_{j+(i-1)k} - \bar{x_i})^2\right) + \frac{size + 2n}{size}, \tag{4.10}$$

where n is the number parameters in the model used, that is, the number of segments in which the signal is divided in; k denotes the length of the segment of which $\bar{x_i}$ is the mean value of the i^{th} segment; and *size* is the total of samples the signal contains, in other words, the sum of all values of k.

Given a set of candidate models, i.e. different segmentations of the signal, the preferred model is the one that produces the minimum AIC value. Therefore, signal segmentation, allied to AIC's classification and selection procedure, is expected to be a good tool for representing a signal simply but also accurately, facilitating the detection of important structural changes.

4.2.4 Event detection algorithm

To correctly classify a segment as a BP event in accordance to the requirements described in 4.1, an algorithm was developed in the form of a non-parametric test, in other words, a test that requires "few if any assumptions about the shapes of the underlying population distributions", as defined by M. J. Campbell [42]. Consequently, the algorithm is developed considering examples of computable metrics from a segmented signal, as depicted in Fig. 4.4.

For a given segment, a set of values can be calculated based on previous segments. These values can then be analysed, in order to explore if a tendency for a drop or rise in BP has been observed in the last 30 min, and if it has been a meaningful one. Fig 4.4 represents the values computed to flag a segment as a BP event. Additionally, the concept of *seen* segments is also represented. These are the segments the currently segment being analysed "remembers", that is, those segments that evaluate the last 30 minutes of the signal, in respect to, and including, the current segment. Considering only recordings of a duration of 1 hour, *seen* segments are represented by a maximum of $\frac{n}{2}$ segments, for a segment numbered over or equal to $\frac{n}{2}$.

The algorithm used for event detection and flagging, for establishing the GT and searching for events in the estimated BP signals (tier 2 function *eventDetection* used in tier 1 functions *groundTruth()* and *estimatedDetection()* of steps 2 and 4 of Table 4.1, respectively) are presented in the form of a flowchart. It receives a segmented signal as input, that is, a vector of numeric values representing each segment of the signal. It then proceeds to process each segment, returning a vector the same size as the input vector, containing 1 or 0 if a segment has been evaluated as an event or not, respectively.

The flowchart is represented in Fig. 4.5. Fig. 4.6 depicts a secondary layer of detail: functions *GetSeenSegments* and *AnalyseSeenSegments* used in the event detection algorithm, but that are separately defined in order not to visually overload the main flowchart.

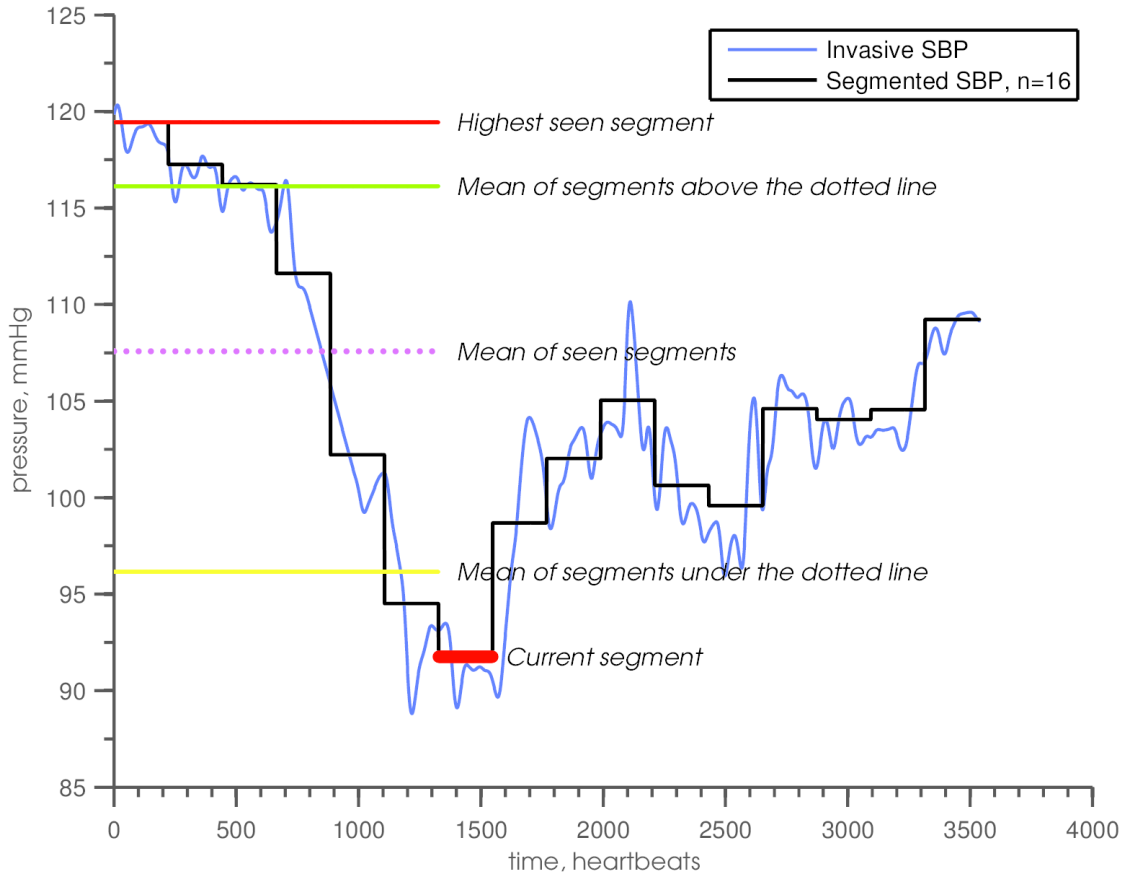

Figure 4.4: Segment evaluation example and values calculated from it.

Variable i represents the position of each of the segments in the input vector; n stands for the number of segments, that is, the vector size; *current* represents the value of the segment currently being evaluated; *nAbove*, $nUnder$, *meanAbove* and $meanUnder$ represent computed values in function *AnalyseSeenSegments* (see Fig 4.6); *threshold* defines the value that needs to be equalled or exceeded to fulfil the second requirement of a BP event (see 4.1); and $Events$ defines the output vector which returns a 1 or a 0 for each segment, if it corresponds to a BP event or not, respectively.

Function *GetSeenSegments* copies from the input vector the *seen* segments. For the sake of simplification we consider only recordings that last 1 hour. Half an hour is consequently defined by $\frac{n}{2}$. So, for each incrementing value of i, while $i <= \frac{n}{2}$, the vector *seen* will grow until it is complete with $\frac{n}{2}$ elements. As i takes values greater than $\frac{n}{2}$, *seen* will contain the last $\frac{n}{2}$ elements in respect to, and including, the *current* segment.

Subsequently, function *AnalyseSeenSegments* computes several values related to the segments in *seen* that will be used to characterize previous segments in respect to the current one. These provide information on whether or not there is a tendency for the rise or fall in BP, and values to calculate if this tendency is large enough to be of relevance, as described in 4.1.

Then, a decision is made based on the those values, for each of the segments:

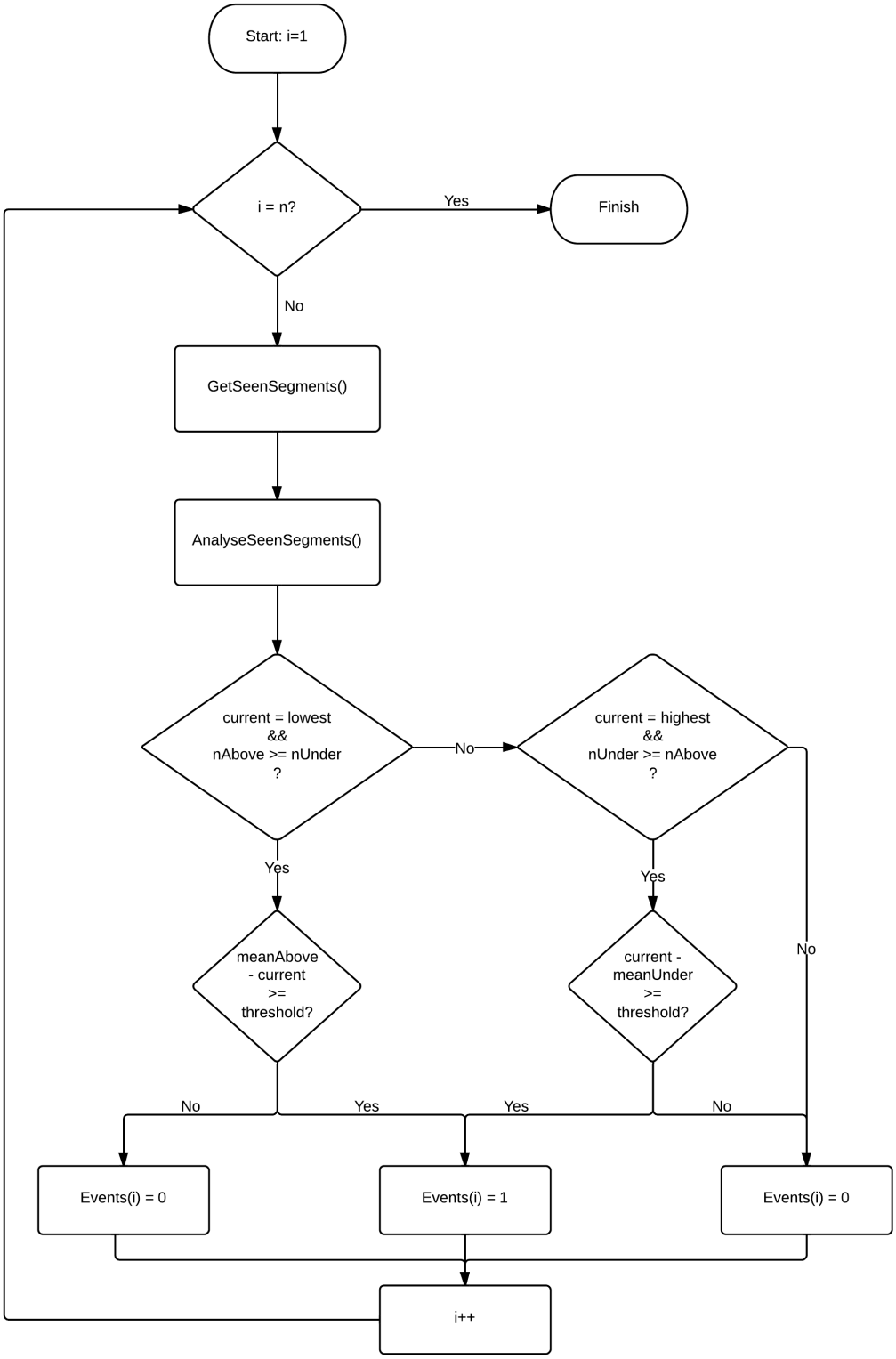

Figure 4.5: Event detection algorithm flowchart.

1. Is there a tendency for a drop in SBP? It is considered so if the *current* segment has the lowest value in *seen* and if the number of elements evaluated above the mean value of *seen* is equal or greater than the number of elements evaluated under.

   (a) If so, go to item 3.

   (b) Else, go to item 2.

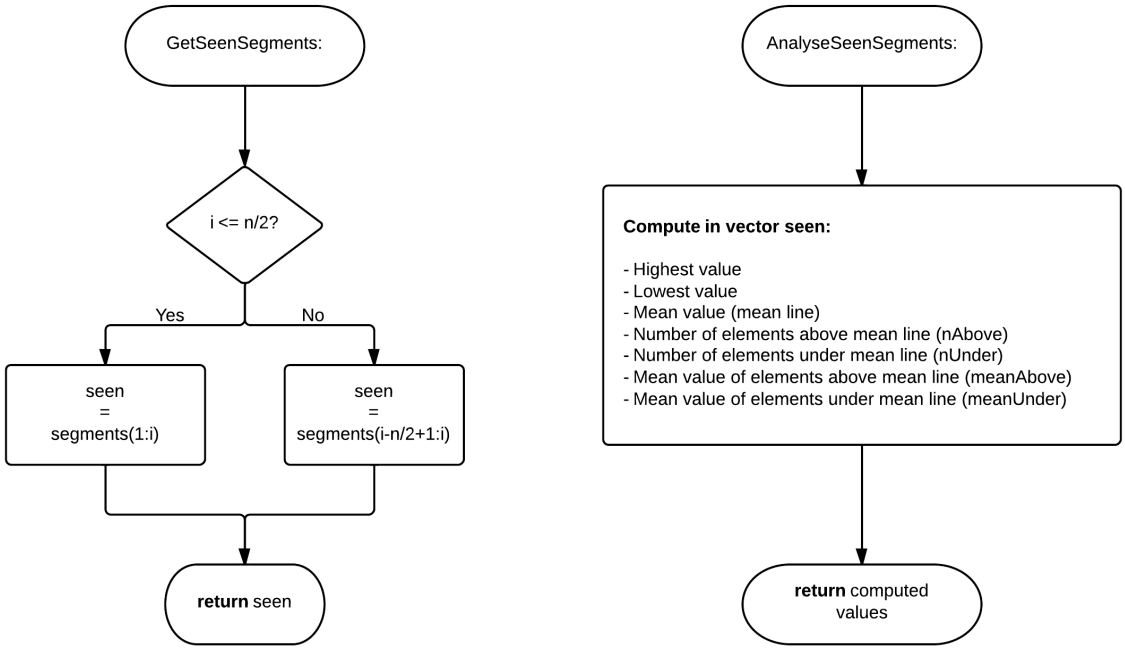

Figure 4.6: Event detection algorithm flowchart.

2. Is there a tendency for a raise in SBP? It is considered so if the *current* segment has the highest value in *seen* and if the number of elements evaluated under the mean value of *seen* is equal or greater than the number of elements evaluated over.

   (a) If so, go to item 3.

   (b) Else, a tendency for a drop or raise in SBP has not been observed.

3. Is the absolute value of the difference between the current segment and the average value of the elements evaluated above or under the mean line, either if decision 1 or 2 is positive, respectively, greater than the threshold defined?

   (a) Yes, this segment is flagged as an event.

   (b) No, the drop or raise was not considerable enough.

This process is applied to all input SBP signals, and the resulting arrays outputted in the form of a struct array instead of a matrix, as these can have different sizes (2, 4, 8, 16, 32, ...) based on the length of the segmented signal, which is determined by the segmentation type (of value p ranging from 1 to p_{max}) which has the lowest AIC .

4.2.5 Processing and comparing events to ground truth

As definition on the duration of a BP event was not provided, alternative ways of processing GT and estimated BP events, were developed so they can be properly compared. The reason for this is that the same event can be detected on consecutive segments, or it can be detected sooner, later or

Underestimation	GT	0	0	0	1	1	1	0	0	0	1	0	0	0
	Events	0	0	0	0	0	1	0	0	0	1	0	0	0
	Result	tn	tn	tn	fn	fn	tp	tn	tn	tn	tp	fn	tn	tn
Overestimation	GT	0	0	0	1	1	1	0	0	0	1	1	0	0
	Events	0	0	0	1	1	1	1	0	0	1	1	1	0
	Result	tn	tn	tn	tp	tp	tp	fp	tn	tn	tp	tp	fp	tn
Delayed Estimation	GT	0	0	0	1	1	1	0	0	0	1	1	0	0
	Events	0	0	0	0	0	1	1	0	0	0	0	1	0
	Result	tn	tn	tn	fn	fn	tp	fp	tn	tn	fn	fn	fp	tn
Advanced Estimation	GT	0	0	0	1	1	1	0	0	0	1	1	0	0
	Events	0	0	1	1	0	0	0	0	1	0	0	0	0
	Result	tn	tn	fp	tp	fn	fn	tn	tn	fp	fn	fn	tn	tn

Table 4.2: Examples where direct comparison of GT and estimated BP event vectors can lead to wrong false positive or negative classifications. *tp*, *tn*, *fp* and *fn* stand for true positive, true negative, false positive and false negative classifiers, respectively. Errors in classification are shown in yellow.

on a less number of segments. Therefore, if the segments were compared directly, several errors could occur that would not translate the real contrast or equality between the two event arrays. Examples of such situations are represented on Table 4.2.

Looking at the *GT* array, it can be seen that it holds two cases where two or more segments are flagged as an event. However, even though there is more than one segment flagged as an event, they are representing the same event. This may take place when an event is of large proportions (in respect to the GT threshold), thus being detected by various segments in a row. In fact, in the four occurrences depicted, the *Events* arrays is able to detect the two events held by the *GT* array, even though it doesn't flag the same sequential segments. Therefore, it needs to be developed a method that re-arranges the arrays in a form that, when comparison takes place, the chances of happening ambiguities like the ones described, are either eliminated or highly reduced.

For this purpose, a simple but effective operation was developed. In table 4.3 are presented the arrays before and after processing the *GT* and *Events* vectors, relatively to the cases provided in 4.2.

GT	Before Processing	0	0	0	1	1	1	0	0	0	1	1	0	0
	After Processing	0	1	0	1	0								
Events	Before Processing Case 1	0	0	0	0	0	1	0	0	0	1	0	0	0
	Before Processing Case 2	0	0	0	1	1	1	1	0	0	1	1	1	0
	Before Processing Case 3	0	0	0	0	0	1	1	0	0	0	0	1	0
	Before Processing Case 4	0	0	1	1	0	0	0	0	1	0	0	0	0
	After Processing	0	1	0	1	0								

Table 4.3: Processing arrays *GT* and *Events* introduced in Table 4.2.

It consists in simply reducing equivalent consecutive flaggings to one, independently of their

length. A sequence of m zeros or ones is transformed in a single zero or one, independently of m being equal to one or the entire length of the array. This is represented in Table 4.4.

		Input											Output
Process Array	Zeros	0	0	0	0	0	0	0	0	0	0	0	0
	Ones	1	1	1	1	1	1	1	1	1	1	1	1
	Alternating	0	1	0	1	0	1	0	1	0	1	0	Equal to input

Table 4.4: Procedure executed by function *processEvents* on binary arrays. Three examples are shown: one array constituted only by zeros, another just by ones and the latter alternates between zeros and ones.

However, each GT, $Events$ pair needs its vectors to have the same length, so a proper comparison takes place. For instance, if a GT vector holds two events and the correspondent $Events$ array only detects one, these will not have the same length. The GT array will have four or five elements (possible combinations 0-1-0-1 or 0-1-0-1-0) and the $Events$ one will have two or three elements (possible combinations 0-1 or 0-1-0). The same can happen if the $Events$ array flags more events than the GT vector holds. Therefore, in either case, the vector of smaller length needs to be extended in order to equal the length of its correspondent. This is done by copying the value of the last element to the extended positions, as exemplified in Table 4.5.

GT Raw	0	0	0	1	1	1	0	0	0	1	1	0	0
Events Raw	0	0	0	1	1	1	1	0	0	0	0	0	0
GT Processed	0	1	0	1	0								
Events Processed without extension	0	1	0										
Events Processed with extension	0	1	0	0	0								

Table 4.5: Example of array extension resulting from different sizes in vectors GT and $Events$.

Given the nature of the data it is not expected that more than two events are detected in the same record. In addition, the first segments will always be evaluated as zero (non-event), as there are not enough *seen* elements to prove a tendency of rise or fall in SBP. So, following detection and processing of events, the resulting array will have usually no more than five elements (0-1-0-1-0), and always at least one element (0), which correspond to scenarios where two events are detected and none are, respectively.

To avoid possible noisy detections an additional requirement was included: events must be spaced at least 20 minutes in time. This feature was also included in processing.

After processing, comparison and classification can take place. Given a $Events$ processed vector, it is multiplied by a factor of 10. Consequently, each element on $Events$ is of value 0 or 10. Given the equivalent GT vector, $Events$ is summed to GT producing an array containing elements of value 0, 1, 10 and 11. It is then possible to classify the events detected from SBP estimated signals relatively to the respective ground truth. This procedure is represented on Table 4.6.

As the first element in an events vector is always a zero (no prior segments are available to exist a tendency – Requirement 1), for event vectors of length greater than one, the first element

Element Value	Classifier	Positive/Negative Count
0	True Negative	+1 Negative
1	False Negative	+1 Positive
10	False Positive	+1 Negative
11	True Positive	+1 Positive

Table 4.6: Classification of elements in an array resulting from the sum of GT and $10 \times Events$.

was chosen not to add to the negative count. The objective here is to not influence the negatives count by adding cases that could never be classified as positive.

Once this process has been applied to the entire set of data and all GT, $Events$ pairs are generated, true positive and false positive rates can be calculated, among other important performance metrics. This, in turn, will produce a point in ROC space. By applying this procedure, using the same GT vectors and recalculating the $Events$ arrays for thresholds varying from ∞ to 0 ideally, many points on ROC space will be obtained. A curve in ROC space can then be generated by applying a fitting curve on these points.

However, the threshold that produces a GT that allows for higher rates of sensibility and specificity needs to be studied by inspecting the data and which events have been flagged either in the GT vector and in its correspond $Events$ array. This subject and other results will be investigated in the next section.

4.3 Results

In this section the results of applying the methods previously described to 69 records of 4 different datasets are presented and discussed.

First, two SBP event detection, one precise and one inaccurate, are to illustrate fluctuation on the quality of the model as an indicator of variability in SBP.

Secondly, ROC performance curves are given for SBP event detection using three distinct methods for estimating SBP. This is done by varying the threshold parameter in the event detection algorithm from, ideally, ∞ to 0. Estimated events vectors for the three different approaches are compared to the ground truth reference vector, creating a point in ROC space for each value of threshold used. Subsequently, the more important points in each of the ROC curves are identified and analysed in terms of sensitivity, specificity, accuracy and precision.

Ultimately, based on figures and tables presented, considerations are made on efficiency, relevance and usability of the BED technique.

SBP is estimated using Model 1 – PTT_{peak}, and signal segmentation uses $p_{max} = 4$, unless stated otherwise.

4.3.1 Results of signal estimation and event detection

From ground truth formation, resulted 24 positive and 74 negative detections. SBP is estimated using the LSF method and events are searched after segmentation of the estimated signal. This

action is performed to all records, using a threshold equal to the one used to generate the ground truth, that is $tr_{gt} = 20$. The resulting segmented invasive and estimated SBP signals, and corresponding non-processed event vectors are then graphically represented. By visual inspection of these graphs for each record, one observes that there are cases where the estimated segmented signal resembles the invasive segmented signal, cases where there is partial resemblance, and cases where there is no resemblance at all.

Figures 4.7 and 4.8 are two illustrative examples of precise and inaccurate resemblance and their event vectors, respectively.

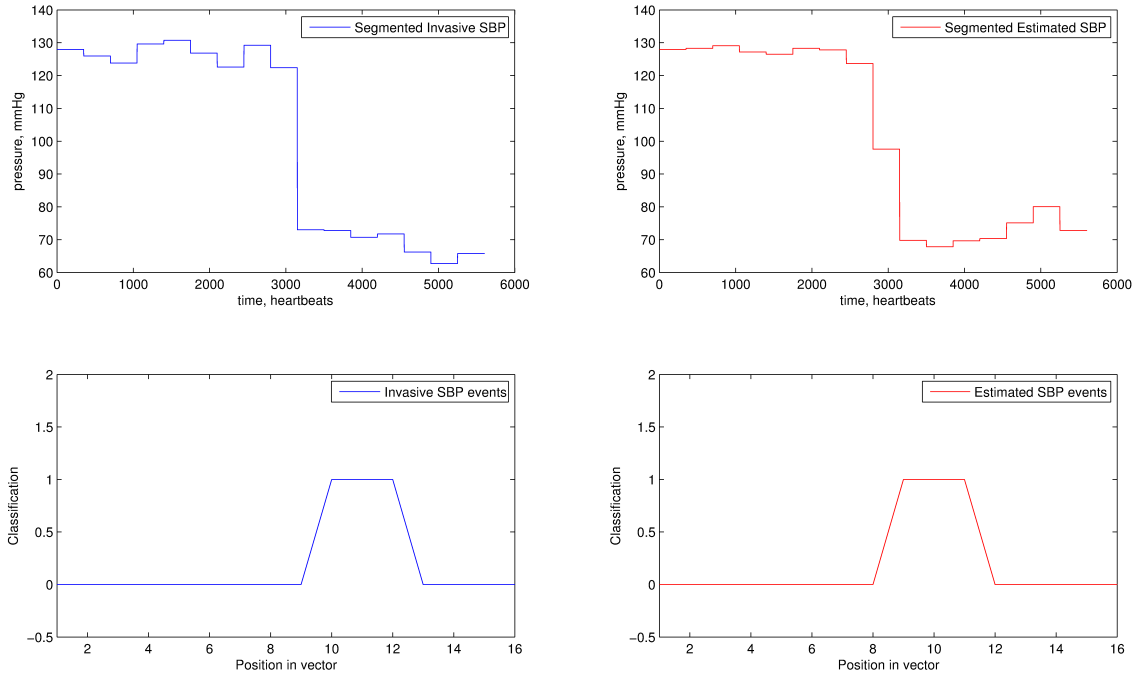

Figure 4.7: Example where good resemblance of invasive and estimated SBP signals leads to an accurate event detection.

Close similarity was found in 10 records, which led to 5 out of 7 existing events detected. Partial similarity was found in 39 records, which led to 3 out of 7 existing events detected. Non existing or few resemblance was found in 20 records, which led to 0 out of 10 existing events detected. A low number of true detections indicates that lower thresholds might give higher true positive rates. But at what cost in return, i.e. false positive rate?

Therefore, it is relevant to ask the question: which are the thresholds that maximize the trade-offs between the number of true and false positive detections? This question will be addressed below.

4.3.2 ROC performance curves results

Figure 4.9 depicts the ROC performance curves for three different SBP estimating methods: *Least Squares Fitting* (LSF), *initial calibration only*, i.e. using the parameters determined by LSF from the first 5 minutes of each record, and EWR with period of $T = 20$ min between re-calibrations.

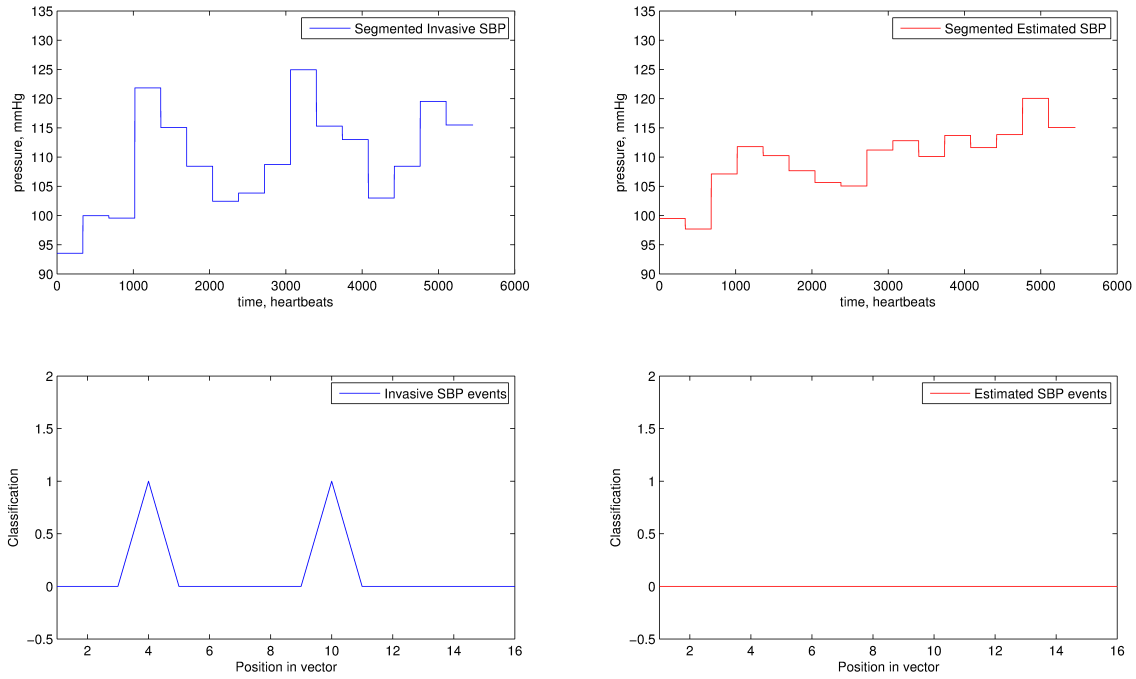

Figure 4.8: Example where bad resemblance of invasive and estimated SBP signals leads to missed event detection.

Threshold was varied between 80 and 0 by a rate of -0.5. Area Under the Curve (AUC) is maximized by the LSF method denoting a better overall performance. Still, the 7 points of more significance in each of the curves are represented in Tables 4.7, 4.8, 4.9, in conjunction with the threshold value applied, for each of the methods.

	SBP Event Detection by Least Squares			
Threshold (mmHg)	**Sensitivity**	**Specificity**	**Accuracy**	**Precision**
$Tr = 20.0$	0.318	1.00	0.844	1.00
$Tr = 18.0$	0.409	0.974	0.847	0.818
$Tr = 17.0$	0.455	0.949	0.840	0.714
$Tr = 12.5$	0.636	0.881	0.830	0.583
$Tr = 10.5$	0.777	0.833	0.821	0.531
$Tr = 8.5$	0.864	0.776	0.792	0.463
$Tr = 0.5$	0.955	0.518	0.552	0.146

Table 4.7: Important performance points in BED *Least Squares* ROC curve.

Points of better *sensitivity/specificity* performance for *LSF*, *Initial Calibration only*, *EWR(T=20)* occur around values of $Tr_{LSF} = 10.5$ *or* 8.5, $Tr_{calib} = 11$ *or* 7.5 and $Tr_{ewr} = 12.5$, respectively. These values are around half the value used for obtaining the GT, $Tr_{GT} = 20$, confirming the issues raised in the previous subsection.

Although the *LSF* method for estimating SBP can not be applied in on-line BP measurement systems, the other two methods could be implemented in a BED monitor that could be incorporated with already existing technology, such as ABPM devices that measure blood pressure at regular

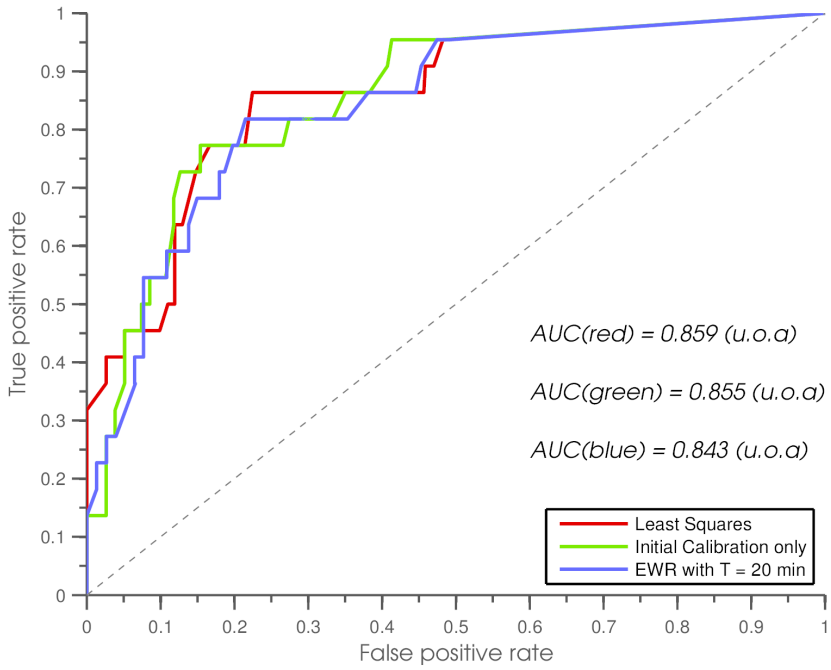

Figure 4.9: ROC performance curves for SBP event detection using three methods of estimating SBP: *LSF*, *initial calibration only*, i.e $EWR\ (T = \infty)$, and $EWR\ (T = 20)$. Used $p_{max} = 4$ for signal segmentation, and $Model1 - PTT_{peak}$ as the SBP estimation model.

	SBP Event Detection by Initial Calibration only			
Threshold (mmHg)	**Sensitivity**	**Specificity**	**Accuracy**	**Precision**
$Tr = 46.0$	0.273	0.974	0.816	0.750
$Tr = 35.5$	0.455	0.949	0.840	0.714
$Tr = 19.5$	0.545	0.915	0.837	0.632
$Tr = 14.5$	0.727	0.874	0.844	0.593
$Tr = 11.0$	0.773	0.846	0.832	0.548
$Tr = 7.5$	0.818	0.726	0.741	0.367
$Tr = 3.0$	0.955	0.587	0.630	0.233

Table 4.8: Important performance points in BED *Initial Calibration only* ROC curve.

	SBP Event Detection by EWR ($T = 20$ min)			
Threshold (mmHg)	**Sensitivity**	**Specificity**	**Accuracy**	**Precision**
$Tr = 50.5$	0.272	0.973	0.814	0.750
$Tr = 43.5$	0.409	0.921	0.806	0.600
$Tr = 36.0$	0.545	0.923	0.840	0.667
$Tr = 18.5$	0.682	0.851	0.817	0.536
$Tr = 12.5$	0.818	0.787	0.793	0.474
$Tr = 5.5$	0.864	0.619	0.652	0.264
$Tr = 2.0$	0.955	0.526	0.569	0.184

Table 4.9: Important performance points in BED *EWR (T = 20 min)* ROC curve.

intervals, e.g. 20 minutes, providing extra, more complete functionalities. Yet, it is important to confirm and reproduce these results on a more vast set of data, with a larger number of positive and negative instances.

Chapter 5

Conclusions and future work

5.1 Fulfilment of objectives

In this work the following questions were answered or partially-answered:

> *How does a PTT-based model perform as an estimator of SBP?*

Several methods were used to approach this question. By applying least squares fitting off-line, low correlation coefficients between the parameters a and b of Model 1 – PTT_{peak} were found. Furthermore, several examples indicated that lower minimum squared error does not imply better curve fitting. By applying recursive least squares off-line, parameters a and b evolution in time was obtained, but no systematic components were observed. This fact indicates that the model holds too little physical information to take into account all the factors that can influence and cause variations is BP. Ultimately, by applying exponentially-weighted regression on-line with re-calibration period T, standard deviation of the error and minimum squared error were observed to increase considerably with T, suggesting that θ_0 (calculated in the initial calibration) becomes increasingly obsolete within a certain period of time. This period has been observed to be about 30 minutes to 1 hour.

> *Is a PTT-based model an indicator of variability strong enough to detect most events of SBP?*

This question was addressed by developing a set of techniques for SBP event detection, where events are characterized by medical requirements suggested by Dr. Vasco Gama and Daniel Caeiro, namely a threshold for significant SBP changes of 20 mmHg. This threshold was applied both in generating the ground truth and detecting events from estimated SBP signals. Low sensibility results indicated that lower thresholds might give better performance rates. This introduced a subsequent question:

> *Which are the thresholds that maximize the tradeoffs between the number of true and false positive detections?*

To study this, ROC performance curves were generated for three different methods of estimating SBP. Important performance points were depicted and analysed. Specific points in EWR($T = 20$) ROC curve suggested that the method could be incorporated with current technology for ambulatory BP measurement using a threshold of $tr = 12.5$ and providing reasonable performance (82% sensibility and 79% specificity). Yet, the results need to be reproduced using a larger set of data.

All in all, initial expectations were met and a contribution has been made, even though results took a different form from that initially defined.

5.2 Future work

Several issues were raised during the development of this work.

A study on circadian variation of the parameters of Model 1 – PTT_{peak} needs to be initiated to observe if there is any effect of the time of the day on parameter value and variation. A method should be developed to determine more objectively and accurately the resemblance between estimated and invasive SBP signals. Robust techniques, such as restraining parameter value, must be developed in order to diminish the impact of noisy measurements on re-calibrations. This may lead to a larger time period between the need for re-calibrations, as the one observed by Cattivelli and Garudadri (2009) [27], of about 1 hour and 20 minutes.

Alternative versions of the event detection algorithm applied need be developed to explore other approaches to signal segment classification. The duration of a BP event should be defined more precisely near medical references, and the method for comparing event vectors will be enhanced based on that characteristic. A larger set of data must be collected to reproduce the results depicted by the ROC performance curves.

References

[1] F.A. Ferreira Marques, D.M.D. Ribeiro, M.F.M. Colunas, and J.P. Silva Cunha. A real time, wearable ecg and blood pressure monitoring system. In *Information Systems and Technologies (CISTI), 2011 6th Iberian Conference on*, pages 1 –4, june 2011.

[2] D.M.D. Ribeiro, M.F.M. Colunas, F.A.F. Marques, J.M. Fernandes, and J.P.S. Cunha. A real time, wearable ecg and continous blood pressure monitoring system for first responders. In *Engineering in Medicine and Biology Society,EMBC, 2011 Annual International Conference of the IEEE*, pages 6894 –6898, 30 2011-sept. 3 2011. doi:10.1109/IEMBS.2011.6091736.

[3] World Health Organization. World health statistics 2012, 2012. URL accessed on 03-02-2013. URL: http://www.who.int/gho/publications/world_health_statistics/EN_WHS2012_Full.pdf.

[4] Thomas G. Pickering, John E. Hall, Lawrence J. Appel, Bonita E. Falkner, John Graves, Martha N. Hill, Daniel W. Jones, Theodore Kurtz, Sheldon G. Sheps, and Edward J. Roccella. Recommendations for blood pressure measurement in humans and experimental animals: Part 1: Blood pressure measurement in humans: A statement for professionals from the subcommittee of professional and public education of the american heart association council on high blood pressure research. *Circulation*, 111(5):697–716, 2005. arXiv: http://circ.ahajournals.org/content/111/5/697.full.pdf+html, doi:10.1161/01.CIR.0000154900.76284.F6.

[5] J.I. Aivars et al Z. Marcinkevics, M. Greve. Relationship between arterial pressure and pulse wave velocity using photoplethysmography during the post-exercise recovery period. In *Acta Universitatis Latviensis*, volume 753, pages 59–68, 2009.

[6] Peter M Rothwell. Limitations of the usual blood-pressure hypothesis and importance of variability, instability, and episodic hypertension. *The Lancet*, 375(9718):938 – 948, 2010. URL: http://www.sciencedirect.com/science/article/pii/S0140673610603091, doi:10.1016/S0140-6736(10)60309-1.

[7] G. Mancia. Prognostic value of long-term blood pressure variability: the evidence is growing. *Hypertension*, 57(2):141–143, Feb 2011.

[8] Peter M Rothwell, Sally C Howard, Eamon Dolan, Eoin O'Brien, Joanna E Dobson, Bjorn Dahlöf, Peter S Sever, and Neil R Poulter. Prognostic significance of visit-to-visit variability, maximum systolic blood pressure, and episodic hypertension. *The Lancet*, 375(9718):895 – 905, 2010. URL: http://www.sciencedirect.com/science/article/pii/S014067361060308X, doi:10.1016/S0140-6736(10)60308-X.

[9] G. J. Langewouters, J. J. Settels, R. Roelandt, and K. H. Wesseling. Why use finapres or portapres rather than intraarterial or intermittent non-invasive techniques of blood pressure measurement? *Journal of Medical Engineering and Technology*, 22(1):37–43, 1998. arXiv:http://informahealthcare.com/doi/pdf/10.3109/03091909809009997, doi:10.3109/03091909809009997.

[10] B.P McGrath. Ambulatory blood pressure monitoring. *Med. J. Aust.*, 176(12):588–592, 2002. URL: http://www.ncbi.nlm.nih.gov/pubmed/12064958.

[11] C.H. Chan and Y.T. Zhang. Continuous and long-term arterial blood pressure monitoring by using h-shirt. In *Information Technology and Applications in Biomedicine, 2008. ITAB 2008. International Conference on*, pages 267 –269, may 2008. doi:10.1109/ITAB.2008.4570615.

[12] M.F.M. Colunas, J.M.A. Fernandes, I.C. Oliveira, and J.P.S. Cunha. Droid jacket: Using an android based smartphone for team monitoring. In *Wireless Communications and Mobile Computing Conference (IWCMC), 2011 7th International*, pages 2157 –2161, july 2011. doi:10.1109/IWCMC.2011.5982868.

[13] Mohammed Saeed, Mauricio Villarroel, Andrew T. Reisner, Gari Clifford, Li-Wei Lehman, George Moody, Thomas Heldt, Tin H. Kyaw, Benjamin Moody, and Roger G. Mark. Multiparameter intelligent monitoring in intensive care ii (mimic-ii): A public-access intensive care unit database. *Critical Care Medicine*, 39:952–960, May 2011.

[14] Ary L. Goldberger, Luis A. N. Amaral, Leon Glass, Jeffrey M. Hausdorff, Plamen Ch. Ivanov, Roger G. Mark, Joseph E. Mietus, George B. Moody, Chung-Kang Peng, and H. Eugene Stanley. Physiobank, physiotoolkit, and physionet: Components of a new research resource for complex physiologic signals. *Circulation*, 101(23):e215–e220, 2000. URL: http://circ.ahajournals.org/content/101/23/e215.abstract, doi:10.1161/01.CIR.101.23.e215.

[15] R. Shriram, A. Wakankar, N. Daimiwal, and D. Ramdasi. Continuous cuffless blood pressure monitoring based on ptt. In *Bioinformatics and Biomedical Technology (ICBBT), 2010 International Conference on*, pages 51 –55, april 2010. doi:10.1109/ICBBT.2010.5479013.

[16] Matthew Ward and Jeremy A Langton. Blood pressure measurement. *Continuing Education in Anaesthesia, Critical Care & Pain*, 7(4):122–126, 2007. arXiv:http://ceaccp.oxfordjournals.org/content/7/4/122.full.pdf+html, doi:10.1093/bjaceaccp/mkm022.

[17] American Heart Association. Understanding blood pressure readings, 2012. URL accessed on 03-02-2013. URL: http://www.heart.org/HEARTORG/Conditions/HighBloodPressure/AboutHighBloodPressure/Understanding-Blood-Pressure-Readings_UCM_301764_Article.jsp.

[18] M. Nitzan. Automatic noninvasive measurement of arterial blood pressure. *Instrumentation Measurement Magazine, IEEE*, 14(1):32 – 37, feb. 2011. doi:10.1109/MIM.2011.5704808.

[19] Y. Hata, H. Muratani, Y. Kimura, K. Fukiyama, Y. Kawano, T. Ashida, M. Yokouchi, Y. Imai, T. Ozawa, J. Fujii, and T. Omae. Office blood pressure variability as a predictor of acute myocardial infarction in elderly patients receiving antihypertensive therapy. *J Hum Hypertens*, 16(2):141–146, Feb 2002.

[20] D.P. Veerman. *Clinical Studies on Blood Pressure Variability*. Universiteit van Amsterdam, 1994. URL: `http://books.google.pt/books?id=6_fGtgAACAAJ`.

[21] G. Parati, R. Casadei, A. Groppelli, M. Di Rienzo, and G. Mancia. Comparison of finger and intra-arterial blood pressure monitoring at rest and during laboratory testing. *Hypertension*, 13(6 Pt 1):647–655, Jun 1989.

[22] G. Parati, A. Frattola, M. Di Rienzo, and G. Mancia. Blood pressure variability. importance in research and in clinical hypertension. *Arq. Bras. Cardiol.*, 67(2):131–133, Aug 1996.

[23] Ben Gupta. Invasive blood pressure monitoring, 2007. URL accessed on 03-02-2013. URL: `http://update.anaesthesiologists.org/wp-content/uploads/2009/09/Invasive-Blood-Pressure-Monitoring.pdf`.

[24] John Allen. Photoplethysmography and its application in clinical physiological measurement. *Physiological Measurement*, 28(3):R1, 2007. URL: `http://stacks.iop.org/0967-3334/28/i=3/a=R01`.

[25] J. Fortin and et al Marte. Continuous non-invasive blood pressure monitoring using concentrically interlocking control loops. *Comput. Biol. Med.*, 36(9):941–957, Sep 2006.

[26] P.A. Shaltis, A.T. Reisner, and H.H. Asada. Cuffless blood pressure monitoring using hydrostatic pressure changes. *Biomedical Engineering, IEEE Transactions on*, 55(6):1775 –1777, june 2008. `doi:10.1109/TBME.2008.919142`.

[27] F.S. Cattivelli and H. Garudadri. Noninvasive cuffless estimation of blood pressure from pulse arrival time and heart rate with adaptive calibration. In *Wearable and Implantable Body Sensor Networks, 2009. BSN 2009. Sixth International Workshop on*, pages 114 –119, june 2009. `doi:10.1109/BSN.2009.35`.

[28] D.B. McCombie, A.T. Reisner, and H.H. Asada. Adaptive blood pressure estimation from wearable ppg sensors using peripheral artery pulse wave velocity measurements and multichannel blind identification of local arterial dynamics. In *Engineering in Medicine and Biology Society, 2006. EMBS '06. 28th Annual International Conference of the IEEE*, pages 3521 –3524, 30 2006-sept. 3 2006. `doi:10.1109/IEMBS.2006.260590`.

[29] M.Y.M. Wong and Y.T. Zhang. The relationship between pulse transit time and systolic blood pressure on individual subjects after exercises. In *Distributed Diagnosis and Home Healthcare, 2006. D2H2. 1st Transdisciplinary Conference on*, pages 37 –38, april 2006. `doi:10.1109/DDHH.2006.1624791`.

[30] M. Y. Wong, C. C. Poon, and Y. T. Zhang. An evaluation of the cuffless blood pressure estimation based on pulse transit time technique: a half year study on normotensive subjects. *Cardiovasc Eng*, 9(1):32–38, Mar 2009.

[31] Parry Fung, G. Dumont, C. Ries, C. Mott, and M. Ansermino. Continuous noninvasive blood pressure measurement by pulse transit time. In *Engineering in Medicine and Biology Society, 2004. IEMBS '04. 26th Annual International Conference of the IEEE*, volume 1, pages 738 –741, sept. 2004. `doi:10.1109/IEMBS.2004.1403264`.

[32] PS Pandian, K Mohanavelu, KP Safeer, TM Kotresh, DT Shakunthala, Parvati Gopal, and VC Padaki. Smart vest: Wearable multi-parameter remote physiological monitoring system. *Medical engineering & physics*, 30(4):466–477, 2008.

[33] P. Bonato. Wearable sensors/systems and their impact on biomedical engineering. *Engineering in Medicine and Biology Magazine, IEEE*, 22(3):18 –20, may-june 2003. doi:10.1109/MEMB.2003.1213622.

[34] M. Sun and R. Jones. Accuracy relationship of blood pressure devices between the aami sp 10 standard and the british hypertension society protocols. *Biomed Instrum Technol*, 33(1):62–70, 1999.

[35] A.H. Sayed. *Fundamentals of Adaptive Filtering*. Wiley, 2003. URL: http://books.google.pt/books?id=VaAV4uqMuKYC.

[36] D. S. G. Pollock. Recursive estimation in econometrics. *Computational Statistics & Data Analysis*, 44:37–75, 2003. doi:10.1016/S0167-9473(03)00150-6.

[37] Tom Fawcett. An introduction to roc analysis. *Pattern Recogn. Lett.*, 27(8):861–874, June 2006. URL: http://dx.doi.org/10.1016/j.patrec.2005.10.010, doi:10.1016/j.patrec.2005.10.010.

[38] Ya Xue, N.H.W. Eklund, Xiao Hu, and Weizhong Yan. Time receiver operating characteristic (troc) curves: A new tool for evaluating the performance of diagnostic systems. In *Neural Networks (IJCNN), The 2010 International Joint Conference on*, pages 1–7, 2010. doi:10.1109/IJCNN.2010.5596675.

[39] David S Stoffer. Walsh-fourier analysis and its statistical applications. *Journal of the American Statistical Association*, v86(n414):p461(19), 1991-06-01.

[40] H. Akaike. A new look at the statistical model identification. *Automatic Control, IEEE Transactions on*, 19(6):716–723, 1974. doi:10.1109/TAC.1974.1100705.

[41] R.H. Shumway and D.S. Stoffer. *Time Series Analysis And Its Applications: With R Examples*. Springer Texts in Statistics. Springer-Verlag GmbH, 2006. URL: http://books.google.pt/books?id=J-moNKkSNrEC.

[42] M.J. Campbell. *Statistics at Square One*. Wiley, 2011. URL: http://books.google.pt/books?id=p727CF-d8zcC.